Floating offshore wind potential for Mediterranean countries

Heliyon 10 (2024) e33948

Contents lists available at ScienceDirect

Heliyon

journal homepage: www.cell.com/heliyon

Research article

Floating offshore wind potential for Mediterranean countries

E. Faraggiana *, A. Ghigo, M. Sirigu, E. Petracca, G. Giorgi, G. Mattiazzo, G. Bracco

Marine Offshore Renewable Energy Lab (MOREnergy Lab), Department of Mechanical and Aerospace Engineering, Polytechnic University of Turin, 10129 Torino, Italy

ARTICLE INFO

Keywords:
Floating wind
LCOE
Wind farm
Renewable energy
Wind turbines

ABSTRACT

Floating offshore wind is a promising renewable energy source for several Mediterranean Countries. The exploitation of this resource will contribute to reducing carbon dependence and support *the clean energy transition towards a climate neutral Europe. This work presents a novel methodology for estimating spatially-resolved Levelised Cost of Energy and offshore wind energy potential to provide optimal design of floating offshore wind farms in the Mediterranean Sea. For the first time, each site is optimised based on electrical grid cable design and wind farm layout optimisation using the Jensen wake model. The largest technical capacity potentials are obtained in Libya, Tunisia, Italy and Greece, accounting for 72.2 % of the total Mediterranean potential with a total installed capacity of* 782 GW. *The average LCOE is 93.4 €/MWh and the average capacity factor is 31.8 %, while 67.5 % of the technical potential has LCOE below 90 €/MWh which demonstrates that floating offshore wind in the Mediterranean could become soon competitive with other renewable energies. Optimal floating wind farm design parameters show the prevalence of a wind farm array of 10x10 wind turbines with a preferred rated power of* 15 MW *and the HVDC export cable connection. Among the selected floating platforms, Hywind outperforms WindFloat and GICON-SOF in 59.2 % of the suitable areas due to the lower structure material. Policymakers and stakeholders will primarily benefit from this study, which provides them with important information for careful marine spatial planning and the development of floating offshore wind farms in the Mediterranean.*

1. Introduction

European Union has targeted an economy based on a net zero greenhouse gas emissions by 2050 [1]. A Renewable Energy Directive in Europe has been proposed since 2009 (2009/28/EC) [2] to increase the share of renewables across the different sectors of economy. The Directive was revised in 2018 (2018/2001/EU) and in 2022 (REPowerEU plan [3]). The REPowerEU plan aims to accelerate the clean energy transition and reduce the EU's dependence on Russian fossil fuels proposing to reach 45 % of renewable energies' share in 2030. Investigating future scenarios for the renewable energy mix is important to reduce variability, increase the reliability of energy systems and properly plan storage capacity [4]. Offshore wind renewable energy in Europe is foreseen to increase to reach the 2030 renewable energy goal. The European Commission has proposed a EU strategy on offshore renewable energy (COM(2020)741) [5], which proposed an offshore wind installed capacity of 60 GW and 300 GW in 2030 and 2050, respectively. In 2022, European offshore wind's cumulative installed capacity was 28.4 GW [6]. However, the Mediterranean region lacks a common regulatory framework for

* Corresponding author.
E-mail addresses: emilio.faraggiana@polito.it (E. Faraggiana), alberto.ghigo@polito.it (A. Ghigo), massimo.sirigu@polito.it (M. Sirigu), ermando.petracca@polito.it (E. Petracca), giuseppe.giorgi@polito.it (G. Giorgi), giuliana.mattiazzo@polito.it (G. Mattiazzo), giovanni.bracco@polito.it (G. Bracco).

https://doi.org/10.1016/j.heliyon.2024.e33948
Received 29 August 2023; Received in revised form 26 June 2024; Accepted 1 July 2024
Available online 2 July 2024

offshore wind development and there are many policy drivers across Mediterranean Countries. For example, the Interreg Maestrale project [7] identified the main legislation applied in eight Mediterranean countries demonstrating the complexity and diversification between them.

An accurate estimation of the offshore wind energy potential will support policymakers and investors in planning an energy strategy and investments in suitable regions around the planet. Global and European offshore wind potentials have been estimated with large uncertainty (50–3200 EJ/y for global, 12–144 EJ/y for European), mainly due to the different resolution of wind speed data, different assumptions of wind farm power density (2–12 MW/km^2) and wind resource constraints (5–8 m/s minimum average wind speed, 20 % minimum capacity factor) as shown in Table 1. Few studies only have also optimised the wind farm design (array spacing) [8], wind turbine rated power, and hub height [9] to obtain more realistic total technical resource potential predictions. However, in Dupont et al. [8] array placement efficiency does not depend on the wind resource and is based only on array spacing and size.

The Mediterranean area is characterised by an increasing interest in offshore wind energy development due to the large potential of the floating offshore wind technology. Bottom-fixed offshore wind is mainly limited to a small region of the Adriatic Sea and was estimated by the European Commission report [10] to be about a hundred times lower than the floating offshore wind potential (46.3 TWh/y for bottom-fixed and 4582.6 TWh/y for floating wind). A lower estimation of the Mediterranean offshore wind potential was obtained in Pantusa et al. [11] (742 TWh/y), due to the inclusion of three depth until 500 m compared to 1000 m of the European report [10].

Country-level offshore wind potential has been also investigated to provide more effective national energy planning guidelines for the most suitable sites for each country [18–22]. These studies can be more detailed in the definition of all constraints (e.g. Ref. [21]) compared to global and European studies and represent a careful techno-economic analysis as a function of water depth, distance to ports, and grid substations [18].

The most suitable locations for floating offshore wind farm projects in the Mediterranean Sea are identified based on wind data analysis and levelized cost of energy. Satellite wind data analysis and regional climate simulations revealed promising areas in the Gulf of Lions and the Aegean Sea [23,24]. In Martinez et al. [25], LCOE was mapped for the Mediterranean Sea, with the lowest values of about 95 €/MWh for the most energetic sites, i.e. the Gulf of Lion. In Caglayan et al. [9] it is shown that LCOE in Europe will reach even lower values (70 €/MWh) by 2050, with 38 % of the sites having an LCOE below 60 €/MWh. LCOE was also used to assess the feasibility of renewable energy farms such as floating offshore wind farms and hybrid wind-wave farms off the coast of Brindisi [26]. LCOE obtained was high (>250 €/MWh), which was justified by the small size of the farm and the wind turbine considered.

Offshore wind farm development for Mediterranean islands has also been investigated, as these are often non interconnected to the mainland and would benefit from an independent energy system. In Onea et al. [27], the most suitable sites of the major Mediterranean islands for offshore wind farm development were characterised based on average wind data and the area located between Corsica and Sardinia, the northern-western part of Crete, and the northern and southern parts of Cyprus were identified. The development of offshore wind farms on smaller islands such as Samothrace and Santorini has been also investigated [28,29]. This showed that the profitability is rather limited due to the small size of the offshore wind farms (e.g. 12 MW [29]).

Current projects, Initiatives, and Programmes (e.g. the WestMED initiative and the Interreg Euro-MED Programme) underline the importance of offshore renewables for mitigating climate change and developing a blue and sustainable economy. Maritime spatial planning (MSP) is essential for the harmonious integration of human activities and the preservation of the environment. Most Mediterranean Countries have not yet adopted a MSP strategy and therefore it is essential to develop tools to support the decision-making process [30]. Existing tools (e.g. Maestrale's WebGIS tool [31], ORECCA's WebGIS tool [32], Global Wind Atlas [33], and New

Table 1
Summary of main assumptions made in previous studies.

	Global	European	Mediterranean
Resolution timeseries (km)	~25 (NOAA) [12], ~50 (GEOS 5, MERRA 2) [13,14], ~80 (ERA-Interim) [8]	~25 (ERA-40, NOAA) [12,15], ~50 (MERRA 2) [9,13], ~80 (ERA-Interim) [8]	~25 (NOAA) [10], ~40 (MERRA) [11]
Resolution average (km)	1 (GWA) [13]	0.25, 1 (Corine Land Cover, GWA) [13,15]	
Energy potential (EJ/y)	50 [8], 565 [14], 694 [12], 1186 [13], 2262 [16], 3200 [17]	12 [8], 122 [15], 141 [13], 144 [9]	3 [11], 16 [10]
Min/max distance to shore (km)	0/93 [12,14]	15/- [9]	8 [11], 22/200 [10]
Maximum depth (m)	200 [12,14], 1000 [8,13]	50 [15], 1000 [8,9,13]	500 [11], 1000 [10]
Wind turbine (MW)	1.5 [16], 3.5 [12], 2.5–3.6 [14], 5 [13]	5 [13], 8 [15], 3–20 [9]	3–6.15 [11]
Power density (MW/km^2)	3.1 [13], 5 [12], 2–10 [8], 5.8–8.9 [14], 9 [16], 9.1 [17]	3.1 [13], 2–10 [8], 12 [15]	1.1–3.6 [11], 7 [10]
Aerodynamic array efficiency (%)	10-99 [8], 89 [13], 90 [12,14]	10-99 [8], 89 [13], 90 [15]	90 [10]
Minimum wind speed (m/s)	6.9 [16]	5 [15]	8 [10]
Minimum capacity factor (%)	20 [12–14]	20 [13]	–
Optimised design parameters	Array spacing [8]	Rated power [9], hub height [9], foundation [9]	–

European Wind Atlas [34]) lack the evaluation of the offshore wind farm productivity and did not consider important MSP resource limitations (e.g. human activities).

This study aims to inform policymakers and stakeholders about techno-economic details and suitable areas for floating offshore wind farm development in the Mediterranean Sea providing further optimal design parameters compared to other studies and including more accurate techno-economic results. The optimal design of offshore wind farms is limited to few studies and there is a lack of an integrated multi-parameter optimisation including several design parameters such as wind turbine and floating platform design, electrical cable design and array design. Furthermore, previous studies have assumed constant specific cable cost, linearly dependent mooring length on water depth and constant aerodynamic and electrical efficiency. In this work, electrical cable-specific costs are obtained as a function of section and voltage values, while an optimal grid connection cable design is proposed to respect a defined maximum voltage drop and current along the electrical lines. Mooring costs are based on a preliminary design of the mooring lines estimating their length depending on sea depth through the catenary equations. The novelty of this work is highlighted below.

- The development of a novel methodology capable of including a high spatial (5 km $\times$ 5 km timeseries + 1 km $\times$ 1 km average) and temporal resolution wind resource and a detailed calculation of the wind farm energy production and the wind farm costs such as electrical grid connection, mooring, installation and Operation and Maintenance (OPEX). The energy production for each site of the spatial grid includes for the first time the Jensen wake model to predict accurately the wake losses of the array layout while the grid connection losses are estimated from the electrical cable design and distance from the infrastructures. The high-resolution 5 km $\times$ 5 km timeseries is the highest one compared to previous studies (not less than 25 km as shown in Table 1).
- The provision of the Mediterranean spatially-resolved LCOE, floating offshore wind potential and several optimal design parameters such as wind turbine rating, floating platform type, AC/DC export cables, wind farm layout, and spacing. Optimal wind farm layout and export cable connection have not been addressed in other studies yet.
- The investigation of the optimal technical resource potential is represented for each Mediterranean country and with respect to the shore distance and water depth, identifying the suitable areas, installed capacity, capacity factor and LCOE.

This paper first describes in Section 2.1 the methodology used for the floating offshore wind resource assessment for the Mediterranean Sea, while Section 2.2 describes all datasets. Floating offshore wind turbines are presented in Section 2.3 and the offshore wind farm modelling and grid transmission losses are described in Section 2.4 and Section 2.5 respectively. The techno-economic analysis is shown in Section 2.6. The results of the study include the verification of the in-house wake model in Section 3.1, the

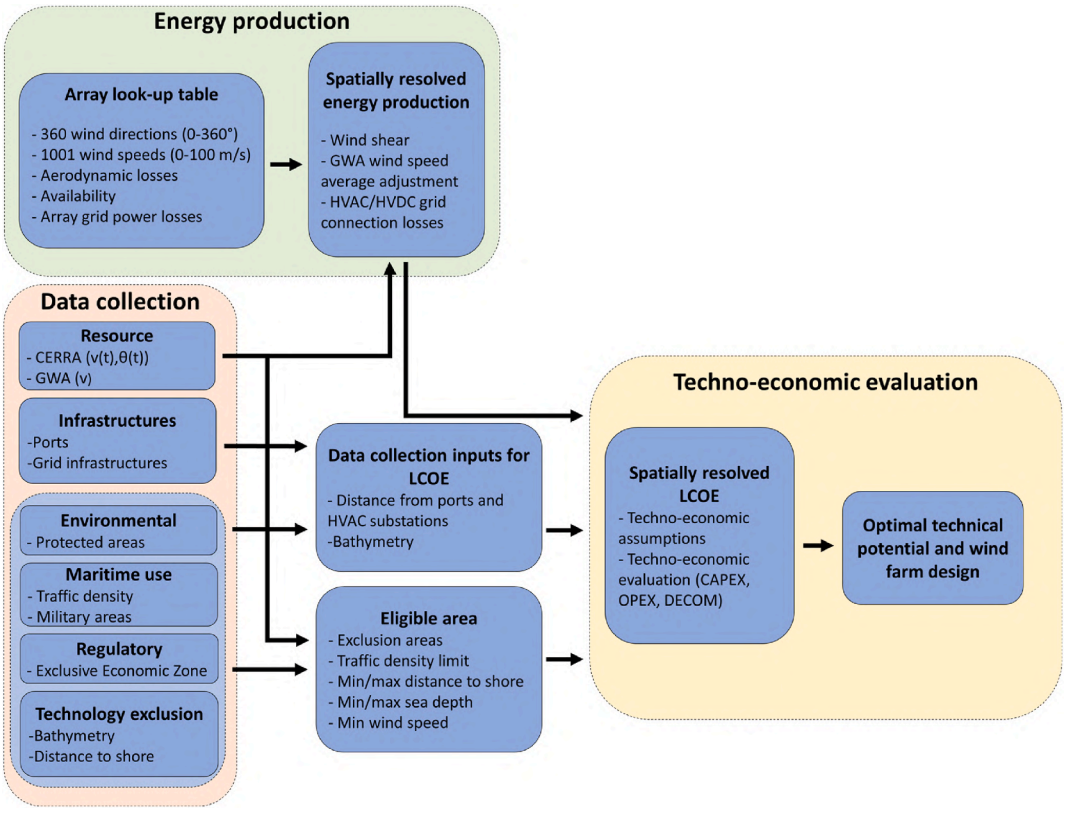

Fig. 1. Methodology to assess the optimal technical potential for Mediterranean countries and the optimal offshore wind farm design. (2-columns image).

influence of siting parameters in Section 3.2, the LCOE sensitivity analysis in Section 3.3 and the optimal floating offshore wind farm design parameters and technical resource potential in Section 3.4 and 3.5 respectively. Finally, the discussion and conclusions are given in Section 4 and 0 respectively.

2. Material and methods

2.1. Methodology

This study developed a methodology shown in Fig. 1 and is used to estimate the technical floating offshore wind potential and LCOE for the Mediterranean Sea by identifying the optimal wind farm layout and spacing, wind turbine, floating platform and HVAC/HVDC grid connection. The optimal LCOE is selected from the LCOE evaluation of two different regular wind farm layouts (5 rows x 5 columns and 10 rows x 10 columns wind turbine array configurations), 27 array spacings, two turbine types (NREL 5 MW and IEA 10 MW) and three floating wind platforms (spar, semi-submersible and TLP). The inputs for the LCOE calculation are the energy production, the distance from ports and HVAC substations, the bathymetry and several techno-economic assumptions described in Section 2.6. The techno-economic evaluation as well as the energy production are spatially-resolved but the first is limited to an eligible area to estimate the technical potential and therefore includes several exclusion areas. The wind farm energy production is calculated from the wind resource timeseries data and includes aerodynamic and electrical power losses (see Sections 2.4 and 2.5) for each array layout, spacing and wind turbine. In this study, the wind farm energy production is not computed for each floating platform as it is not significantly affected.

2.2. Data collection

Data collected for this study includes the resource, maritime spatial constraints, and infrastructure datasets presented in Table 2, which are mainly used to estimate the energy production, the eligible marine area, and the offshore wind farm cost, respectively. All datasets were discretized in the MATLAB environment to the same resolution of $0.01^\circ \times 0.01^\circ$, and were collected in three formats (.nc, .tiff, and.shp). The first two formats handle array datasets at a given resolution and have been interpolated to obtain the selected accuracy ($0.01^\circ \times 0.01^\circ$). The last format provides a set of vector coordinates that are converted to an array format as they are used to evaluate the eligible area and estimate the technical potential of the Mediterranean countries (Exclusive areas datasets). Datasets of infrastructures include the coordinates of the ports and of the European onshore grid stations. Finally, the distances to the coast, to the nearest port, and to the nearest onshore grid station with a voltage of 220 kV and above are computed in order to verify the required technical constraints (Table 3) and to perform a more accurate techno-economic analysis. For this purpose, the coastline coordinates are obtained from the bathymetry dataset, including the coordinates adjacent to the zero-depth of bathymetry. The Reference ellipsoid for World Geodetic System 1984 is used to compute the distance between the coordinates.

The technical constraints of the floating wind platforms used in this study are listed in Table 3. The minimum and maximum allowable water depths are different for each type of floating platform and were assumed from the Carbon Trust report of 2015 [35]. The spar type requires a larger minimum depth than the other two due to the larger draft but can be deployed in deeper waters. Semi-submersible and TLP have a similar maximum allowable water depth of 400 m. A minimum distance from the coast is required to reduce the visual impact of the offshore wind farms. A minimum distance of 12 km was assumed for the 5 MW wind turbine, similar to Martinez et al. and Westerberg et al. [25,36], while it is increased to 20 km for the 15 MW wind turbines maintaining the same angle of elevation (0.43°). Maximum distance to shore is assumed 200 km, similar to the European Commission report [10], to account for the increased installation, and OPEX costs of an offshore wind project, which are no longer economically viable at very long distances. This constraint is indirectly included in the bathymetry technical constraint, as water depths beyond 200 km from the coast of the Mediterranean Sea are technically prohibitive [33]. Offshore wind potential is also constrained by available resources and is limited by a minimum average wind speed of 4 m/s, similar to Swart et al. [15]. A maximum maritime traffic density (3 (hours/(km^2y)) is also considered to limit the installation of the floating offshore wind farms outside the main traffic routes.

2.2.1. Resource datasets

The European Centre for Medium-Range Weather Forecasts (ECMWF) provides several weather forecast datasets that are reliable

Table 2
Datasets included in this work.

Dataset type	Dataset name	Source	Resolution	File type
Resource	Wind speed and wind direction	CERRA [37]	$0.05^\circ \times 0.05^\circ$	.nc
	Wind speed	GWA [33]	$0.0025^\circ \times 0.0025^\circ$	.tiff
Technical	Bathymetry	GEBCO [38]	$0.0042^\circ \times 0.0042^\circ$	.nc
Maritime use	Maritime traffic	Emodnet [39]	$0.0126^\circ \times 0.0126^\circ$	.tiff
	Military zones	Emodnet	–	.shp
Environment	Protected areas	Emodnet	–	.shp
Regulatory	Exclusive Economic Zones (EEZ)	Emodnet	–	.shp
Infrastructures	Ports	Ports.com [40]	–	–
	Grid infrastructure	PyPSA-Eur [41]	–	.nc

Table 3
Spatial constraints of floating wind platforms.

	Spar	Semi-sub	TLP
Minimum depth (m)	150	50	50
Maximum depth (m)	500	400	400
Minimum distance 5MW/15 MW WT (km)	12/20	12/20	12/20
Maximum distance (km)	200	200	200
Minimum wind speed (m/s)	4	4	4
Maritime traffic density (h/(km^{2}y)	3	3	3

and verified with experimental data [42]. The timeseries of wind speed and direction are obtained from Copernicus European Regional ReAnalysis (CERRA) [37] for the decade 2011–2020 and for a height level of 100 m. The timeseries are 3-hourly distributed and have a resolution of 0.05° × 0.05°. The CERRA dataset has been preferred compared to the other popular ECMWF reanalysis dataset ERA5 since this last has a lower resolution (0.25° × 0.25°). Average wind speeds of the Global Wind Atlas (GWA) [33] ($v_{GWA,100,mean}$) were used to increase the spatial resolution of the CERRA timeseries further to 0.01° × 0.01°. The timeseries with a 0.01° × 0.01° resolution and at a 100 m level ($v_{100}(t)$) is expressed as

$$v_{100}(t) = v_{CERRA,100}(t) \cdot \frac{v_{GWA,100,mean}}{v_{CERRA,100,mean}} \tag{1}$$

In Eq. (1), $v_{CERRA,100}(t)$ and $v_{CERRA,100,mean}$ are the timeseries and the average wind speeds of the CERRA dataset interpolated with a 0.01° × 0.01° resolution.

Average of the ratio between the GWA and CERRA wind speeds is 1.03, while the standard deviation is 0.05 m/s, showing a good agreement between the CERRA and GWA datasets. $v_{GWA,100,mean}$ shown in Fig. 2 have a resolution of 250 m × 250 m but were limited to 0.01° × 0.01° (~1 km × 1 km) in this study similar to all the other datasets.

The wind speed is corrected to account for the hub height position of the wind turbines considered in this study (NREL 5 MW and IEA 15 MW). The logarithmic wind profile, which assumes neutral stability conditions, is used to estimate the wind speed at the hub heights wind turbines' (h_{hub}). It is expressed as

$$v_{hub}(t) = v_{100}(t) \cdot \frac{\ln\left(\frac{h_{hub}}{z_0}\right)}{\ln\left(\frac{100}{z_0}\right)} \tag{2}$$

In Eq. (2), z_0 is the roughness length of the Mediterranean Sea which is 0.0002 m in the offshore environment [33]. v_{hub} is used to estimate the energy production of the offshore wind farm as described in Section 2.4.

2.2.2. Spatial constraints datasets

Spatial constraints datasets were collected to account for the reduction in available marine spatial area due to technical feasibility, human activities, exclusion areas, and exclusive zones (See Fig. 3). The bathymetric dataset shown in Fig. 3a is obtained from the General Bathymetric Chart of the Oceans (GEBCO) which is considered the most important publicly bathymetric dataset of the world oceans [38]. Traffic density, military areas, marine protected areas, and exclusive economic zones shown respectively in Fig. 3b, 3c, 3d and 3e have been collected from the European Marine Observation and Data Network (EMODnet) [39]. EMODnet is a network of

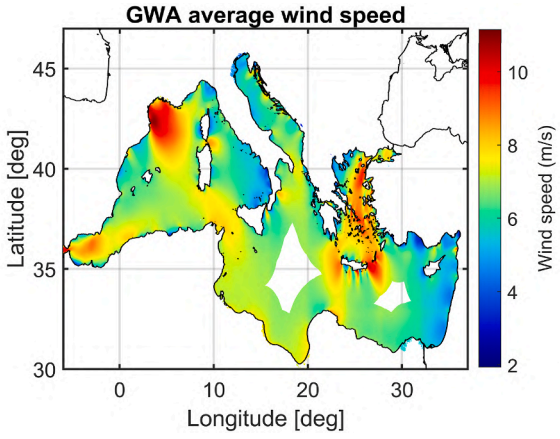

Fig. 2. GWA average wind speed limited to 200 km from the shoreline. (Single column image).

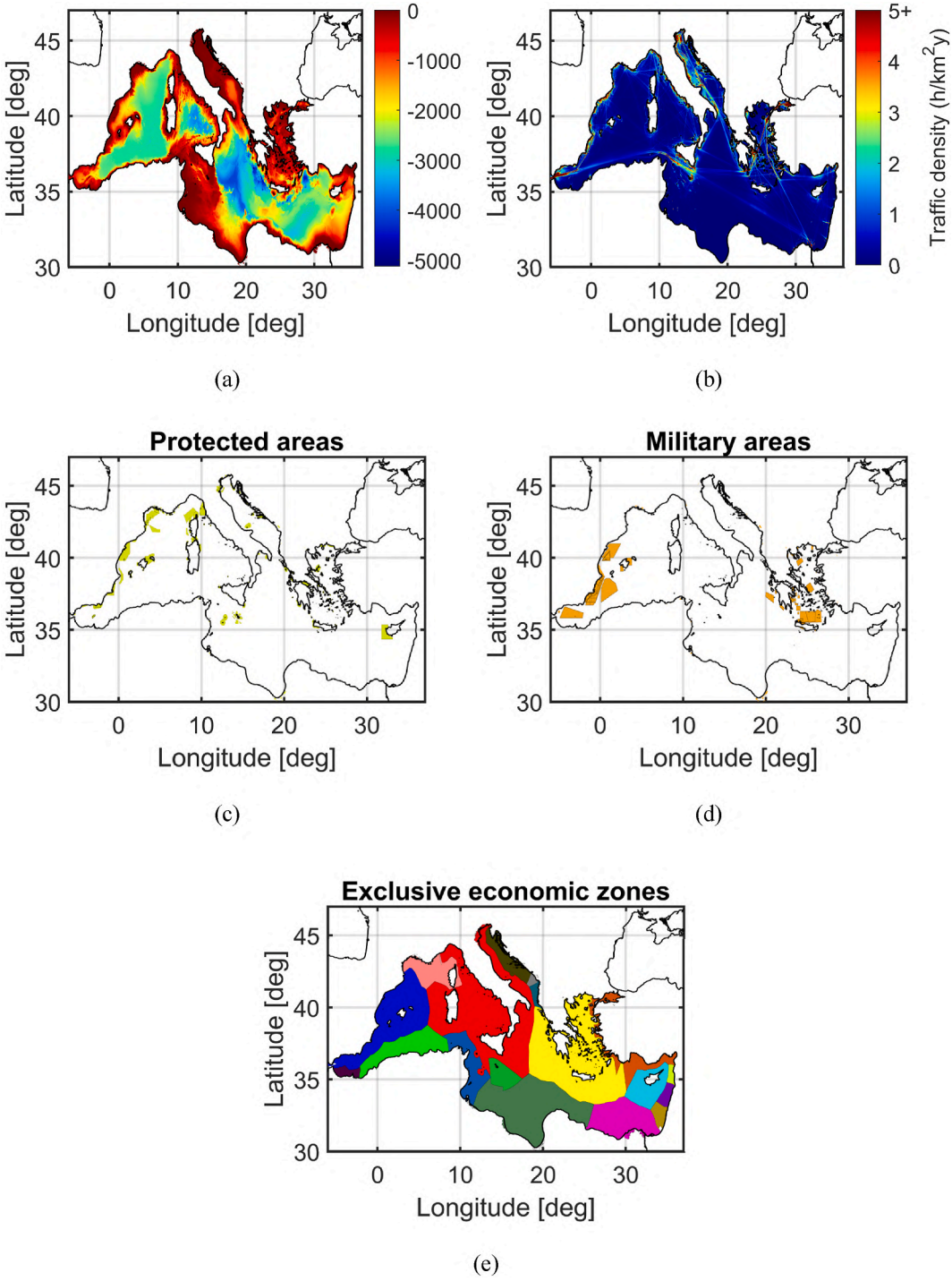

Fig. 3. Visualization of maritime restrictions datasets including bathymetry (a), traffic density (b), protected areas (c), military areas (d) and Exclusive economic zones (e). (2-columns images).

organisations that provides freely available European marine data according to international standards. Traffic density refers to all vessel types, including fishing and passenger vessels. Marine protected areas include the Natura 2000 sites [43], e.i. an ecological network composed of sites designed by the Birds and Habitats Directives in Europe. The dataset of military areas in Europe was created by CETMAR [44] for EMODnet in 2020 and includes military zones in Spain and Greece in the Mediterranean Sea.

2.2.3. Infrastructures datasets

Available infrastructures such as ports and grid infrastructures as shown in Fig. 4a and b respectively, are collected to estimate more accurately the floating offshore wind farm costs due to Operation and Maintenance (O&M), installation, and grid connection costs accounting for the distance from the ports and the HVAC electrical substations. Mediterranean port locations were obtained from Ports.com [40], a global platform that provides information on ports worldwide. Only ports that have a dry dock have been considered in the dataset. The onshore HVAC grid substations were obtained from the open-source dataset PyPSA-Eur [41] maintained and coordinated by the Technical University of Berlin which covers the full European Network of Transmission System Operators for Electricity (ENTSO-E) area [45] and includes substations with a voltage of 220 kV and above. Further substations along the African coast have been included by georeferencing the ENTSO-E grid map in QGIS [46]. The substations of the major Mediterranean islands (Crete, Cyprus, and Rhodes) and some interconnected islands (Balearic and Aegean islands) were also included. The HVAC cable length is derived from the distance between the offshore wind farm and the nearest coastal substation.

2.3. Technology definition

Currently, there are three major types of floating offshore wind platforms [47], distinguished according to the design principle by which they achieve their stability: the buoyancy-stabilized platform (or semi-submersible platform), the mooring-stabilized platform (or tension-leg platform (TLP)) and the ballast-stabilized platform (or spar-platform). The floating offshore wind turbines considered in this study are Hywind (spar type), WindFloat (semi-submersible type), and GICON-SOF (TLP type), which are shown in Fig. 5a, 5b and 5c respectively.

The NREL 5 MW and the IEA 15 MW are open-source wind turbine models [48] and were selected to investigate the impact of the wind turbine type on the technical floating wind potential in the Mediterranean Sea. Wind turbine thrust coefficients and power values of the wind turbines were determined from the steady-state values of Open-FAST simulations using the ROSCO controller and are shown in Fig. 6.

2.4. Offshore wind farm modelling

The wake deficit of a wind turbine is predicted using Jensen's kinematic model, also known as the PARK model [53,54]. The aerodynamic model includes also an area overlapping rotor-average model and the Sum of Squares (SS) wake interaction model similar to the model already described in Faraggiana et al. [52]. The perturbed wind speed on each wind turbine is determined for 360 wind directions (1° spacing between 0° and 360°) and for 1001 wind speeds (0.1 m/s spacing between 0 and 100 m/s). The wind farm considers two different sizes of 25 and 100 wind turbines in a regular aligned wind farm layout and 27 different wind array spacings (l_s) between 4 and 30 times the wind turbine diameter. The power produced by each wind turbine is calculated using the power curves described in the previous section 2.3 and are saved in a look-up table $P_{iT}(\theta, v, s, m, t)$ as a function of the wind directions (θ) and speeds (v), array size (s) and spacing (m), and wind turbine type (t).

The annual energy production (AEP) of the offshore wind farm is finally calculated in each grid cell as

$$AEP(s,m,t) = \left(\sum_{i_t}^{N_t} \eta_{avail} \sum_{iT}^{N_T} \left(P_{iT}(\theta(t), v_{hub}(t), s, m, t)\right) - P_{EL}(t) \right) \cdot \frac{\Delta t}{n_y} \tag{3}$$

In Eq. (3), N_t is the number of timeseries values for the 10 years considered (2011–2020), η_{avail} is the average availability of the offshore wind turbines, assumed to be 95 % in this study [55], N_T is the number of wind turbines, $P_{EL}(t)$ are the electrical power losses (see

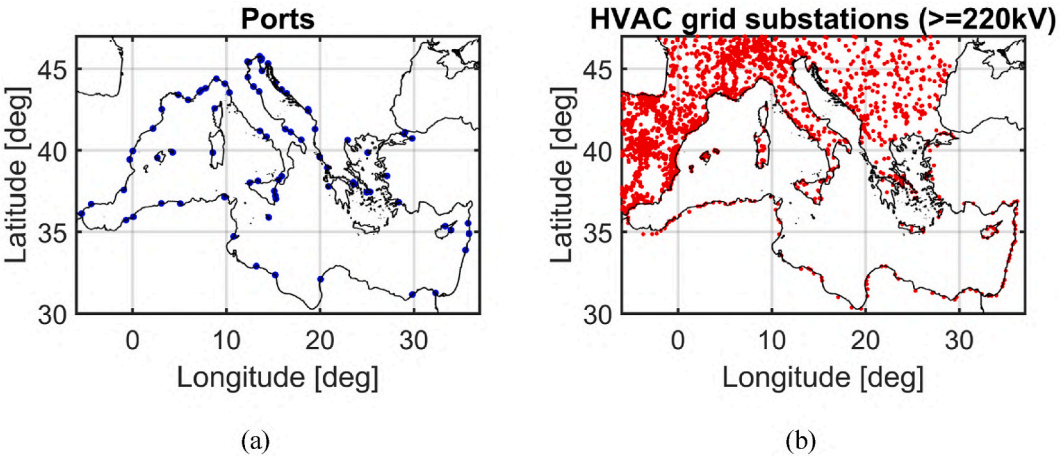

Fig. 4. Available ports and electrical grid substations for the Mediterranean Sea. (2-columns image).

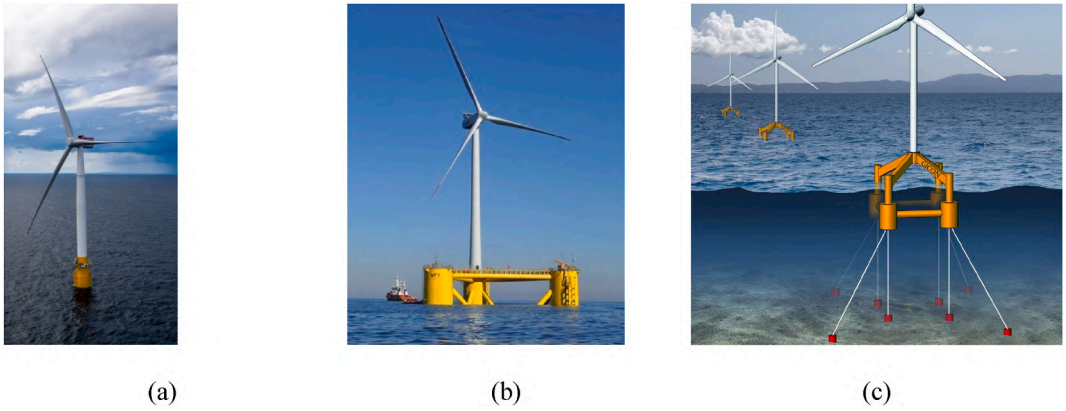

Fig. 5. Photos of the Hywind Scotland floating wind farm (a) and of the WindFloat Atlantic project (b), and rendering of the GICON-SOF (c) [49–51]. (2-columns image).

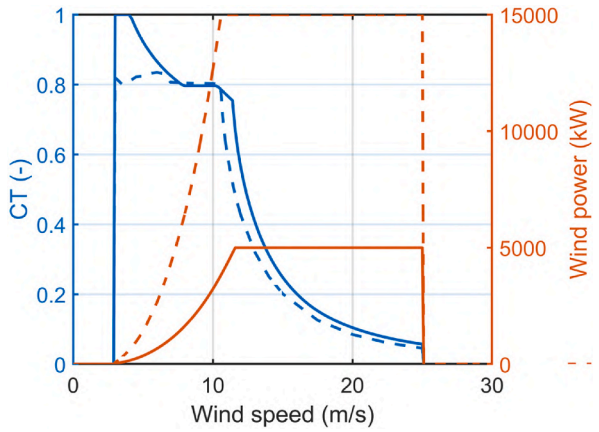

Fig. 6. Thrust coefficients (CT) and wind power of the NREL 5 MW (solid line) and IEA 15 MW (dashed line) [52]. (Single column image).

section 2.5), Δt is the number of hours of each P_{iT} (3 h) and n_y are the number of years.

The capacity factor (CF) of the 5 MW wind turbine and the 5x5 wind farm size is represented in Fig. 7 as a function of the array spacing, wind speeds, and directions. CF is significantly affected by wind speeds up to 15 m/s, as shown in Fig. 7a. Above this speed, CF is not modified by the different wind farm spacing, as the wind speed for all wind turbines is above the rated wind speed. CF is also

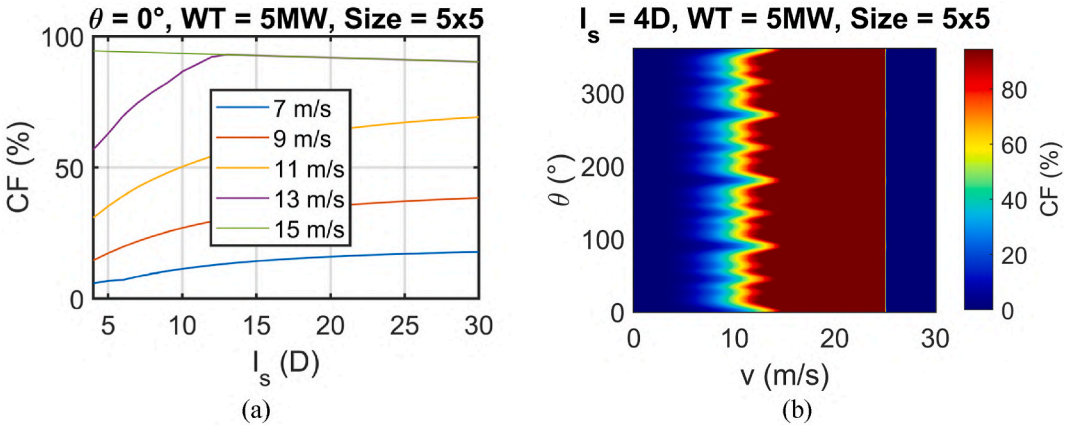

Fig. 7. Capacity factor of the 5 MW wind turbine and 5x5 wind farm size as a function of the wind farm array spacing and wind speeds (a) and of the wind speeds and wind directions (b). (2-columns image).

slightly reduced by increasing the wind farm spacing as the wind farm energy production takes into account the electrical inter-array grid connection losses which increase with spacing. Wind direction influence on CF can be observed in Fig. 7b. The regular aligned wind farm layout gives a similar CF every 90°, as the relative position of the wind farm to the wind direction is the same. The worst CF results are obtained every 90° due to the larger shadowing effect between the wind turbines.

2.5. Grid transmission losses

The electrical grid connection includes the collection and the transmission system. The collection system connects the offshore wind turbines to the offshore substation via a Medium Voltage Alternating Current (MVAC) line (33 kV). The transmission system transfers the power produced collected in the offshore substation to the onshore substation via a High Voltage Alternating Current (HVAC) line or High Voltage Direct Current (HVDC) (220 KV). The electrical grid layouts of the 5x5 and 10x10 offshore wind farm are represented in Fig. 8a and b respectively. For both wind farm sizes considered in this study, a simple radial network was chosen. This type of network is generally selected because it is a cost-effective solution compared to other layout types [56]. The electrical grid layout of the 5x5 offshore wind farm assumes that the offshore substation is located next to the offshore wind turbine in the centre of the farm. Electrical grid connection losses (P_{EL}) are the sum of the electrical losses of the inter-array (P_{IAL}) and export cables (P_{ECL}). The inter-array electrical losses are obtained as

$$P_{IAL}(\mathrm{t}) = 3 \cdot \sum_{i=1}^{N_T} R_{c_i} \cdot I_{c_i}^2(t) \tag{4}$$

In Eq. (4), R_{c_i} and I_{c_i} are the resistance and the instantaneous current of the cable segment.

Power cables selected in this study are 3-core XLPE cables, as they have low manufacturing costs and dielectric losses [56]. The cable resistance is obtained as

$$R_{c_i} = \frac{\rho_{c_i} \cdot \mathrm{L}_{c_i}}{S_{c_i}} \tag{5}$$

In Eq. (5), ρ_{c_i} is the copper resistivity of the cable $\left(1.75 \cdot 10^{-8} \frac{\Omega}{m}\right)$, L_{c_i} is the length of each cable segment and S_{c_i} is the cross-sectional area of the cable.

The three phase AC current of each cable segment can be expressed as [57]:

$$\mathrm{I}_{c_i}(\mathrm{t}) = \frac{P_{c_i}(t)}{\sqrt{3} \cdot V_{MVAC} \cos(\phi)} \tag{6}$$

In Eq. (6), P_{c_i} is the total inter-array instantaneous power in each cable segment, V_{MVAC} is the voltage of the inter-array grid connection (33 kV) and $\cos(\phi)$ is the power factor. A high-power factor equal to 0.95 is assumed in this study for double-fed asynchronous generators according to Bjerkseter et al. and Wildi [57,58].

The section cable (S_c) is obtained by imposing a maximum percentage voltage drop (5 %) and a maximum permissible current.

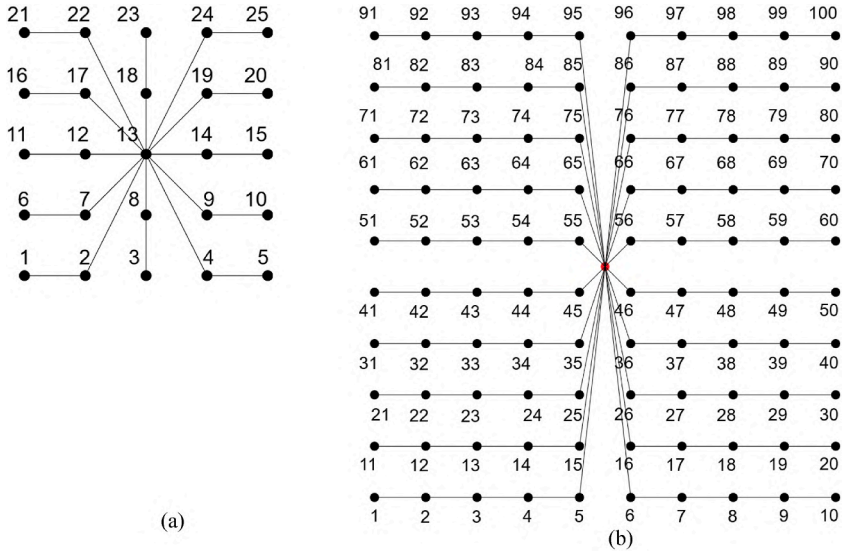

Fig. 8. Inter-array electrical grid connection layout of the offshore wind farm 5x5 (a) and 10x10 (b). (2-columns image).

These values have been obtained from the IEC 60228 standard on conductors of insulated cables [59] and from the catalogue for submarine cables available from Cable Service Srl [60]. The voltage drop is calculated as

$$\Delta V = \sqrt{3} \cdot I_n \cdot L_c \cdot \frac{Z_c}{1000} = \sqrt{3} \cdot I_n \cdot L_c \cdot \sqrt{R_c^2 + X_c^2} \tag{7}$$

In Eq. (7), I_n is the nominal current, Z_c is the impedance of the cable $\left(\frac{\Omega}{km}\right)$ which depends on the conductor resistance and reactance.

The maximum current (I_z) is obtained as follows [60]:

$$I_z = I_{z\,th} * k \tag{8}$$

In Eq. (8), k is a correction factor based on the mean environmental temperature (T_a) and $I_{z\,th}$ is the maximum current at a reference temperature for a specific S_c.

The selected cable cross-sectional area is the smallest section which respects a $\Delta V < 5\%$ and $I_n < I_z$. The look-up tables for conductor and reactance resistance, correction factor (k), and maximum current (I_z) used in this study are shown in Fig. 9a. The conductor reactance is lower than the conductor resistance for cable sections less than 200 mm^2. An example of a selected cable section of line 1–2 for an offshore wind farm 5x5 and a wind turbine of 5 MW is given in Fig. 9b. A cable section is selected for each cable line segment connecting the different nodes of the inter-array layout. Each cable line segment has a different nominal current and cable length, resulting in a differently designed cross-sectional area and resistance.

The methodology for determining the HVAC export cable losses is similar to the inter-array grid connection losses since they are HVAC cables. The HVDC export cable losses are calculated in Eq. (9) as

$$P_{ECL}(t) = 2 \cdot R_{c_{ex}} \cdot I_{c_{ex}}^2(t) \tag{9}$$

while the voltage drop (ΔV) and the instantaneous current ($I_{c_{ex}}$) are obtained in Eq. (10) and Eq. (11) respectively as

$$\Delta V = 2 \cdot I_n \cdot L_{c_{ex}} \cdot \frac{R_{c_{ex}}}{1000} \tag{10}$$

and

$$I_{c_{ex}}(t) = \frac{P_f(t)}{V_{HVAC}} \tag{11}$$

where $P_f(t)$ is the offshore wind farm's total instantaneous power and $L_{c_{ex}}$ is the export cable length.

HVAC power cables include electrical reactance, which becomes more significant compared to conductor resistance as the cable section increases, as shown in Fig. 9. HVDC export cables are more expensive than HVAC for shorter export cable lengths, while they are more advantageous than HVAC for longer distances, as shown for a layout configuration 5x5 in Fig. 10a and for a layout configuration 10x10 in Fig. 10b. Above a certain cable length, larger HVAC sections are required to achieve the maximum allowable voltage drop compared to HVDC.

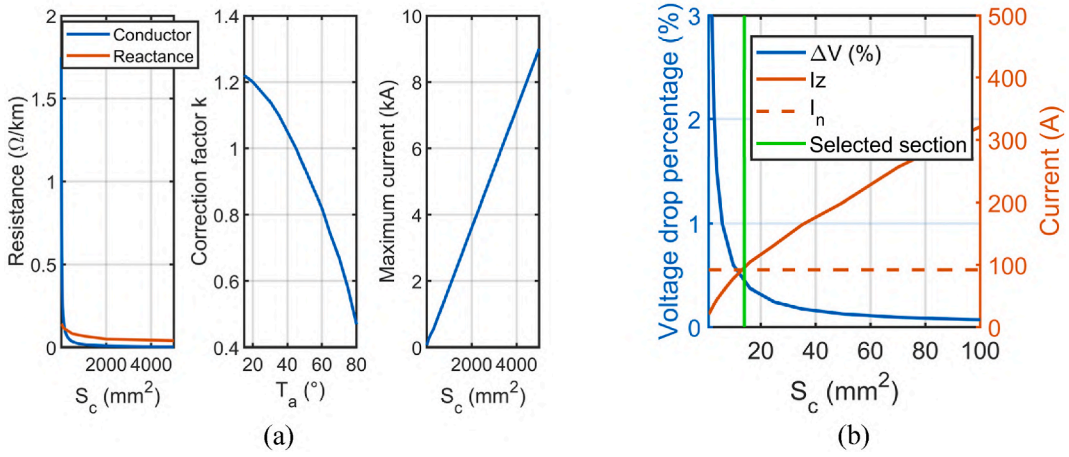

Fig. 9. *Look-up tables for designing the marine cables and an example of selected cross-sectional area of cable line segment 1–2 for the offshore wind farm 5x5, the* 5 MW *wind turbine and 4xD wind turbine spacing. (2-columns image).*

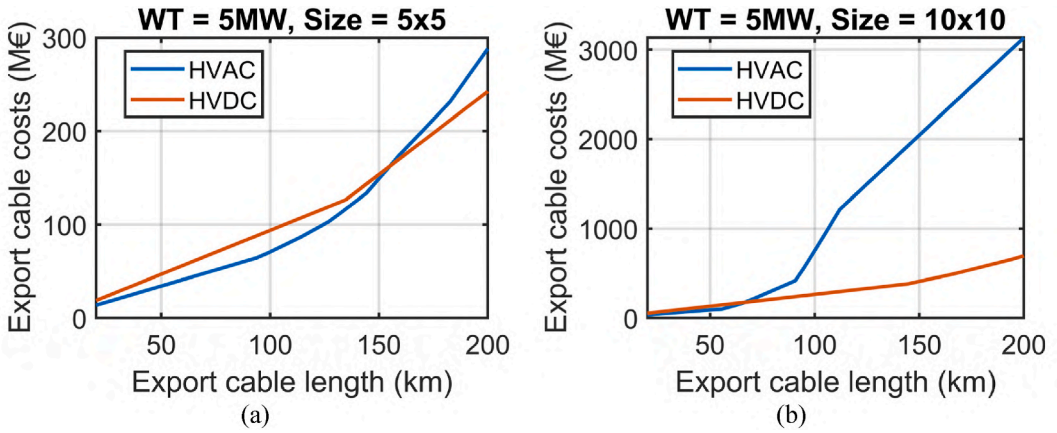

Fig. 10. HVAC and HVDC export cable costs (including installation costs) for the 5 MW wind turbine and an offshore wind farm of 5x5 (a) and 10x10 (b). (2-columns image).

2.6. Techno-economic analysis

2.6.1. LCOE

The Levelised Cost of Energy (LCOE) of the state-of-the-art floating offshore wind concepts is investigated across the Mediterranean as it is a comprehensive Key Performance Indicator (KPI) to assess the most suitable design and locations for energy production [61, 62]. LCOE is expressed similar to Faraggiana et al. [52] with same assumptions of the Weighted Average Cost of Capital (10 %) and the project lifetime (25 years) and it is calculated in each grid cell.

The CAPital EXpenditure (CAPEX) is obtained as

$$CAPEX = C_{Turb} + C_{Plat} + C_{Moor} + C_{Inst} + C_{Grid} \tag{12}$$

In Eq. (12), C_{Turb} is the wind turbines cost including the towers, C_{Plat} is the floating platforms cost, C_{Moor} is the moorings cost, C_{Inst} is the installation cost and C_{Grid} is the grid connection cost.

Specific costs of the floating platforms are 0.51, 0.65, and 0.55 M€/MW for Hywind, WindFloat, and GICON SOF, respectively [35]. A cost reduction factor C_R [63] is accounted for C_{Turb}, C_{Plat} and C_{Moor} to account for the cost reduction in series production and it is expressed in Eq. (13) as

$$C_R = \left(\frac{2}{3} + \frac{1}{3}e^{-0.00174 \cdot N_T^2}\right) \tag{13}$$

C_{Turb} is obtained in Eq. (14) as

$$C_{Turb} = (3 \cdot \log(\mathrm{P_R}) - 0.6624) \cdot \mathrm{N_T} \cdot C_R \tag{14}$$

where $\mathrm{P_R}$ is the wind turbine rated power.

Decommissioning cost is a fraction of the installation cost as it is a reverse installation process which can be performed more easily (See Table 4).

2.6.2. Grid connection cost

Grid connection cost is influenced by the cross-sectional area and voltage and is determined from a cost model developed by Sharkey [56]. It is expressed as

$$C_{Grid} = \sum_{i=1}^{N_T} C_{int_i} + C_{ex} + \mathrm{C_{Offsub}} + \mathrm{C_{Onsub}} \tag{15}$$

Table 4
Decommissioning cost [64].

	% of installation cost
Floating wind turbine	70
Grid subsea cables	10
Substations	90
Mooring	90

In Eq. (15), C_{int} and C_{ex} are the inter-array and export cables costs, C_{Offsub} and C_{Onsub} are the costs of the offshore and onshore substations.

The inter-array cable costs and export cable costs are obtained as

$$\sum_{i=1}^{N_T} C_{int_i} + C_{ex} = \sum_{i=1}^{N_T} \left(C_{refC} \cdot f_{S_i} \cdot f_{V_i} \cdot L_{c_i} \right) + C_{refC} \cdot f_{S_{ex}} \cdot f_{V_{ex}} \cdot L_{c_{ex}} \tag{16}$$

In Eq. (16), C_{refC} is the reference inter-array cable specific cost (200 €/m for 95 mm^2 and 10 kV) and L_{c_i} are the grid connection cable lengths. f_S and f_V are used to correct C_{refC} to account for a different section (f_S) and voltage (f_V) than the given reference and are shown in Fig. 11.

The offshore and onshore substation costs (C_{Offsub}, C_{Onsub}) are estimated as the sum of the transformer and switchgear costs. The transformer cost is obtained in Eq. (17) as

$$C_{tr} = c_{tr1} \cdot P_{farm} \tag{17}$$

where c_{tr1} is assumed as 150.9 k€/MW and 21.56 k€/MW for the offshore and onshore transformer respectively [65] and P_{farm} is the wind farm rated power (MW). The switchgear cost is estimated in Eq. (18) as

$$C_{switch} = c_{s1} \cdot V_{HVAC} + c_{s2} \tag{18}$$

where c_{s1} and c_{s2} are respectively 0.668 €/V and 36 k€ [66].

2.6.3. Mooring cost

The mooring cost (C_{Moor}) is calculated in Eq. (19) as

$$C_{Moor} = n_M \cdot (C_{Anchor} + C_{Mline}) \cdot N_T \cdot C_R \tag{19}$$

where n_M is the number of mooring lines, C_{Anchor} is the anchor cost and C_{Mline} is the mooring line cost. Catenary mooring and chain lines are used for Hywind and WindFloat, while taut-leg mooring and steel wire lines are assumed for GICON-SOF as described in Table 5. The anchor type is difficult to estimate as it requires knowledge of the soil conditions, which is beyond the purpose of this work. Fine sediments are the most typical sediment throughout the Mediterranean Sea, allowing the use of most of the anchor types, including drag and gravity anchors adopted in this study [35,39]. Drag embedded anchors are selected for the Hywind and WindFloat floating wind platforms while GICON-SOF is characterised by a single gravity anchor integrated into the floating platform itself during towing [67]. The mooring line cost of the chain C_{Mline_c} and wire C_{Mline_w} is calculated in Eq. (20) and Eq. (21) respectively as [68]

$$C_{Mline_c} = c_{Mw} \cdot c_{Mc} \cdot L_m \tag{20}$$

and

$$C_{Mline_w} = 0.03415 \cdot d_m^2 \cdot L_m \tag{21}$$

where c_{Mw} (kg/m) and c_{Mc} (€/kg) are the mooring chain specific costs, L_m is the mooring line length (m) and d_m is the mooring wire

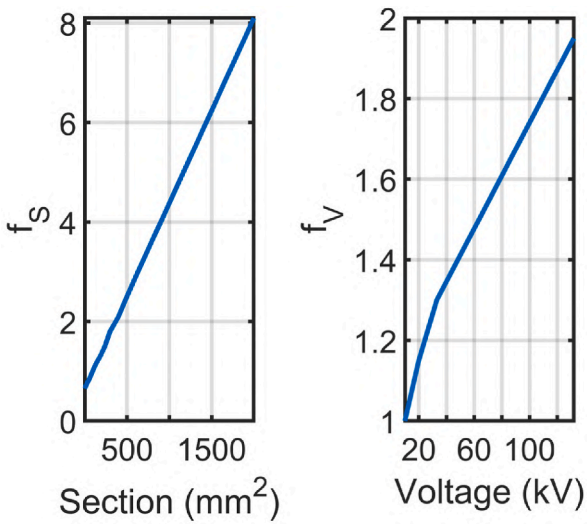

Fig. 11. Correction factors of the inter-array cable specific costs. (Single column image).

Table 5
Mooring details of Hywind, WindFloat and GICON-SOF [35,73,74].

		Hywind	WindFloat	GICON-SOF
Mooring	**Lines**	3	3	4 (main vertical tendons)
	Anchor cost (M€)	0.07	0.07	0.56
	c_{Mc} (€/kg)	2.75	2.75	–
	dm (mm) (5 MW/15 MW)	90/185	90/185	135/247
	MBL (kN) (5 MW/15 MW)	5842/19588	5842/19588	11537/38680
	Radius to fairleads (m)	5.2	32.6	21.9
	Depth to fairleads (m)	70	22.9	30.7
	Mooring type	Catenary, chain	Catenary, chain	Taut, wire

diameter (mm). The mooring chain specific weight c_{Mw} is obtained in Eq. (22) as [68]

$$c_{Mw} = 0.02 \cdot d_m^2 \tag{22}$$

The mooring length (L_m) is obtained as a function of the sea depth and floating platform type. Preliminary mooring designs of Hywind and WindFloat are obtained by using the catenary equations for each mooring line [69]. The minimum mooring length of each line is obtained for the maximum static wind turbine thrust using a safety factor of 1.7, respecting a maximum surge offset of $0.12 \cdot depth$ [70], a negative anchor force, and a maximum mooring line tension less than the Minimum Breaking Load (MBL) [71,72]. All mooring lines are also checked to avoid slack lines for the maximum surge offset. The results of the mooring line length optimisation are shown in Fig. 12. The mooring length is shorter for the 15 MW wind turbine due to the larger mooring line section's diameter, resulting in a larger mooring stiffness. The mooring length is also shorter for Hywind compared to WindFloat due to the deeper mooring fairleads and therefore a shorter distance between fairleads and anchors. Total mooring length of GICON-SOF is obtained as the sum of the four vertical lines connecting the fairleads and the anchors.

2.6.4. *Installation cost*

The main operations required to install the floating wind turbines are described in Table 6. This includes first the installation of the mooring, where the mooring lines and the anchors are attached, followed by the towing of the floating substructure. Hywind and WindFloat assume a similar duration for the installation of the drag-embedded anchors (8 h each), while GICON-SOF incorporates a lowerable gravity anchor into the platform itself, which assumes 32 h of operational time required to install it. The assembled Hywind floater and tower are towed horizontally and erected next to the installation site (1 km distant from the installation site), while WindFloat and GICON-SOF do not include the up-ending operation as they are assembled in the dry dock. Rotor and nacelle are assembled onshore with two lifting operations on the preassembled floater and tower for WindFloat and GICON-SOF, while they are assembled offshore for the Hywind device [64]. Finally, the full floating device is towed to the offshore site and connected to the mooring system. Ballasting of Hywind and WindFloat is completed inshore by a crane barge and two tugs while ballasting of GICON-SOF is made offshore since the attached gravity anchor is ballasted and lowered to the seabed. Towing of the floating wind

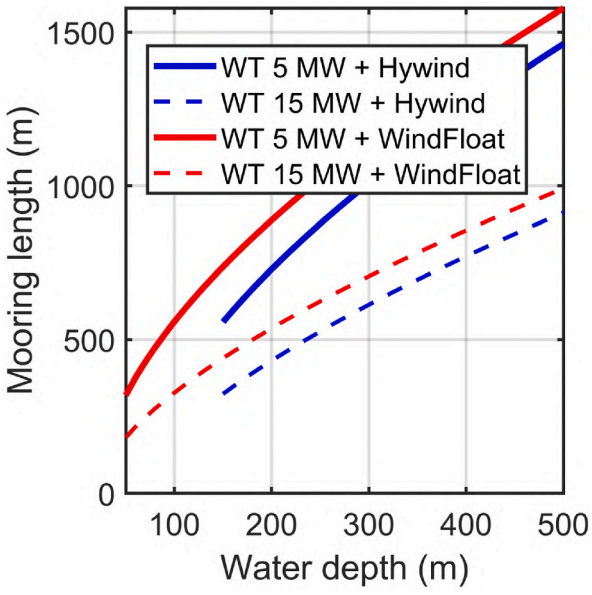

Fig. 12. Mooring length as a function of water depth for Hywind and WindFloat.(Single column image).

Table 6
Installation operations details for each floating wind technology.

Operation	Floating wind	Vessel type	Duration operation (h)	Towing speed (km/h)	OW operation (%)	OW towing (%)
Mooring installation	Hywind	1 AHTS + 2 Tugs	8 for each anchor	27.8	60	75
	WindFloat	1 AHTS + 2 Tugs	8 for each anchor	27.8	60	75
	GICON	1 AHTS + 2 Tugs	32	5.6	60	50
Up-ending	Hywind	1 crane + 2 tugs	12	7.8	60	72
	WindFloat	–	–	–	–	–
	GICON	–	–	–	–	–
Lifting	Hywind	1 crane + 2 tugs	9	7.8	72	72
	WindFloat	1 crane + 2 tugs	9	–	75	–
	GICON	1 crane + 2 tugs	9	–	75	–
Ballast	Hywind	1 crane + 2 tugs	24	7.8	60	72
	WindFloat	1 crane + 2 tugs	24	–	60	–
	GICON	1 crane + 2 tugs	24	5.6	60	50
Mooring connection	Hywind	1 AHTS + 2 Tugs	6 for each line	5.6	55	50
	WindFloat	1 AHTS + 2 Tugs	6 for each line	9.3	55	55
	GICON	1 AHTS + 2 Tugs	–	–	–	–

turbine and mooring operation are carried out by the Anchor Handling Tug Supply (AHTS) and two tugs. Suitable Operational weather Windows (OW) and towing speeds are obtained from Bjerkseter et al. and Myhr et al. [57,64], while vessel costs are given in Table 7.

Grid connection installation costs are obtained using a similar methodology described in Section 2.6.2. They are given as the sum of the inter-array and export cable installation costs and are expressed as

$$C_{Inst_{Grid}} = \sum_{i=1}^{N_T} C_{Inst_{int}} + C_{Inst_{ex}} = \sum_{i=1}^{N_T} \left(C_{refI} \cdot f_{I_i} \cdot L_{c_i} \right) + C_{refI} \cdot f_{I_{ex}} \cdot L_{c_{ex}} \tag{23}$$

In Eq. (23), C_{refI} is the reference inter-array installation cable specific cost (160 €/m for 95 mm^2 and 10 kV) and f_I is the correction factor to consider the influence of section and voltage (f_I).

Substation installation costs (onshore and offshore) are assumed to be 10 % of the substation costs, which is similar to the estimation given in Bjerkseter et al. [57].

2.6.5. Operation and maintenance

Annual maintenance costs include preventive maintenance (3.5 k€/MW) and unplanned corrective maintenance (10.8 k€/MW) [57]. OPEX cost details are obtained from Bjerkseter et al. [57] for an offshore wind farm of 500 MW and include material, labour, vessels, port, and insurance costs. The number of specialised maintenance vessels, maintenance events, and employees have linearly rescaled to the offshore wind farms rated power of this study.

A detailed overview of the specific cost for small and large components is given in Fig. 13. Most of the replacement cost is due to the control and protection system of the generator and the blade adjustment mechanism (pitch hydraulic system).

The cost of the specialised maintenance vessels is assumed 1.9 M€/year for a 500 MW offshore wind farm, while fuel consumption is 1.5 tonnes/day. Total fuel cost is determined by the number of maintenance events per year (assumed 992 for a 500 MW offshore wind farm [57]), the distance of the offshore wind farm from the port, specific fuel cost (640 €/tonne), and the operational weather window (50 %). An offshore crane vessel is employed for major repairs and an operational time of 4 days is assumed for an offshore wind farm of 500 MW at 200 km from the port. Daily cost and fuel consumption of the crane vessel are assumed as 300 k€/day and 48.7 tonnes/day. The costs for the specialised maintenance vessels and the actual operational time of the crane vessel were rescaled to the site-specific offshore wind farm distance and rated power.

Labour costs are listed in Table 8 and describe the number and annual costs for technicians, managers, and administrative staff on a fixed contract basis for a 500 MW offshore wind farm [57]. Offshore technicians are supposed to work for 12 h daylight periods. Personnel costs have been estimated based on UK sector offshore wind energy salaries.

Additional port facilities are required to provide storage and personnel accommodation and it is assumed a cost of 4.8 k€/MW. Finally, the O&M insurance is included in the total O&M cost and it is 17.5 k€/MW.

Table 7
Costs for each vessel type [57].

	Cost (k€/day)
Tug	17
Crane barge	55
AHTS	91

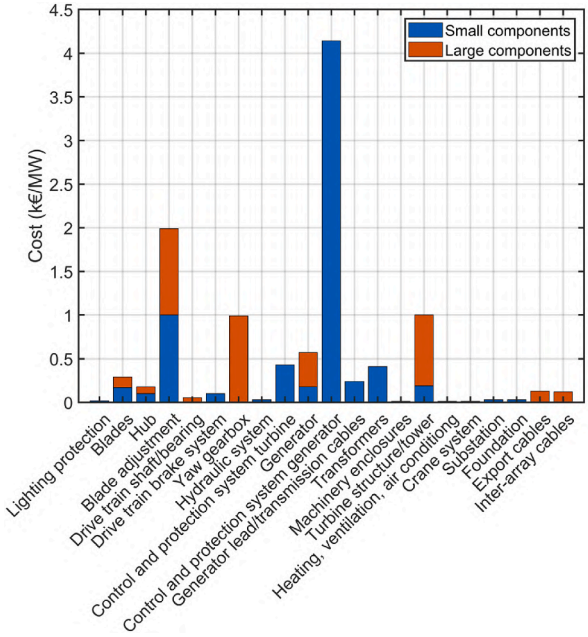

Fig. 13. Material cost of unplanned corrective maintenance [57]. (Single column image).

Table 8
Annual labour cost for a 500 MW offshore wind farm [57].

	Number of employees	Annual cost (k€)
Offshore technicians	60	67
Offshore managers	2	118
Offshore administration	6	60
Onshore technicians	3	50

3. Results

3.1. Wake model verification

The MATLAB-based in-house wake model is verified with Pywake [75] to increase confidence in the offshore wind farm power production estimation. Pywake is a well-known open-source Python code developed by the Technical University of Denmark (DTU) able to estimate the AEP of an offshore wind farm by selecting the wake deficit, superposition, and rotor-average models. The in-house model and Pywake are compared for two different wind farm configurations, three wind directions as shown in Fig. 14a and c for the first and second layout respectively. Fig. 14b and d show the layouts of the two wind farm configurations considered in this verification. Energy production of the wind farm is the largest for the wind direction of 0° for both layouts at a wind direction of 0° and is slightly affected at a wind direction of 60° and more affected at 90°. The first layout (Fig. 14a) is more influenced by the 90° wind direction as the shadowing effect is larger. The in-house code and Pywake show very similar AEP results with a very small relative difference (about 0.0001 %). The in-house code demonstrated a higher computational efficiency (5–6 times faster) compared to Pywake, as Pywake probably simulates several subroutines that slow down the computation. The in-house MATLAB code was chosen for compatibility with the MATLAB code of the resource assessment tool developed in this study and for higher code transparency and flexibility.

3.2. Influence of site parameters

Floating offshore wind farm costs have been investigated as a function of the port distance, the export cable length, and the sea depth for a wind farm of 100 turbines and 15 MW wind turbines (See Fig. 15). Platform and wind turbine costs are not affected by these investigated parameters. The platform costs for each type are only influenced by the specific costs described in Section 2.6.1.

Installation cost and mooring cost are different between the floating platforms. The installation cost of the spar is higher than the semi-submerged mainly due to the up-ending of the floater in the offshore site with a lower operational window and also due to the lower towing speed of the complete floating wind turbine. The installation cost of the TLP is the largest one since the anchor installation and the ballasting is conducted in a single offshore operation mobilising also the crane and not only the tugs and the AHTS.

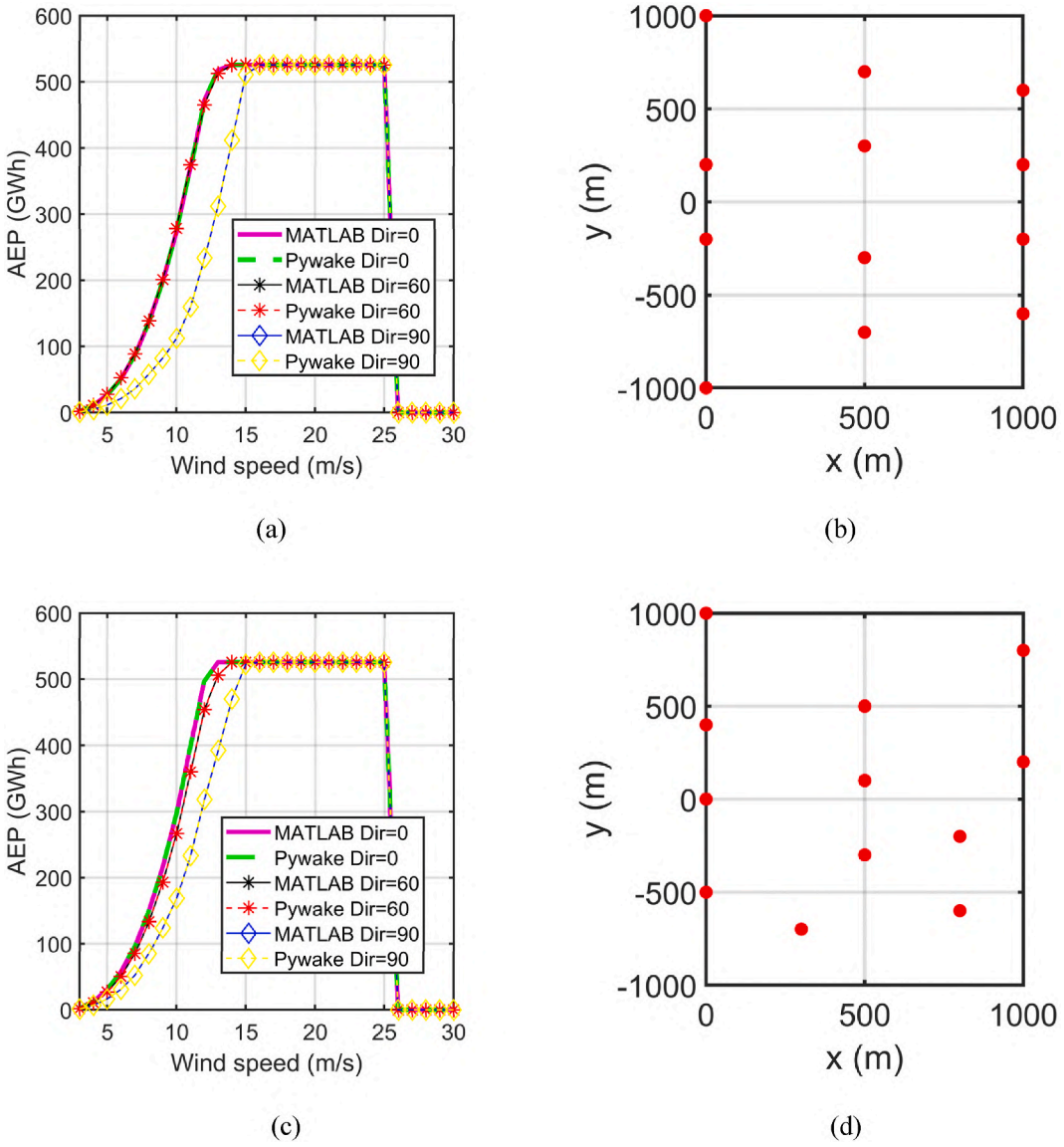

Fig. 14. Verification of the MATLAB in-house code with Pywake for layout 1 (a, b) and layout 2 (c, d). Wind direction is relative to the x axis. (2-columns image).

Mooring costs are similar between the floating platform but the largest ones are for the TLP due to the higher number of lines compared to the other 2 types and the more expensive anchors (4 instead of 3).

The OPEX is influenced by the port distance as the total maintenance time required by the vessels depends on the distance to the offshore wind farm. An increase in the port distance leads in particular to an increase in total rent and total fuel consumption of the vessels.

Port distance and sea depth have a smaller impact on offshore wind farm costs compared to the export cable length. Larger port distances lead to an increase in installation and OPEX costs, while deeper sea depths are associated with an increase in mooring costs. The grid connection and installation costs are instead significantly influenced by the export cable length. Floating offshore wind farms located 200 km from the onshore grid substation have much higher grid connection costs, about 3–4 times larger than an offshore wind farm 20 km distant. Therefore, the location of a floating offshore wind farm should be close to an onshore grid substation.

3.3. Sensitivity analysis

A sensitivity analysis of the LCOE has been carried out to assess the impact of the input parameters as shown in Fig. 16. The LCOE uncertainty could be related to market cost variations associated with the offshore wind farm components (e.g. platform, wind turbine, mooring, grid connection) due for example to the volatility of the steel cost. Furthermore, the installation strategy for each floating

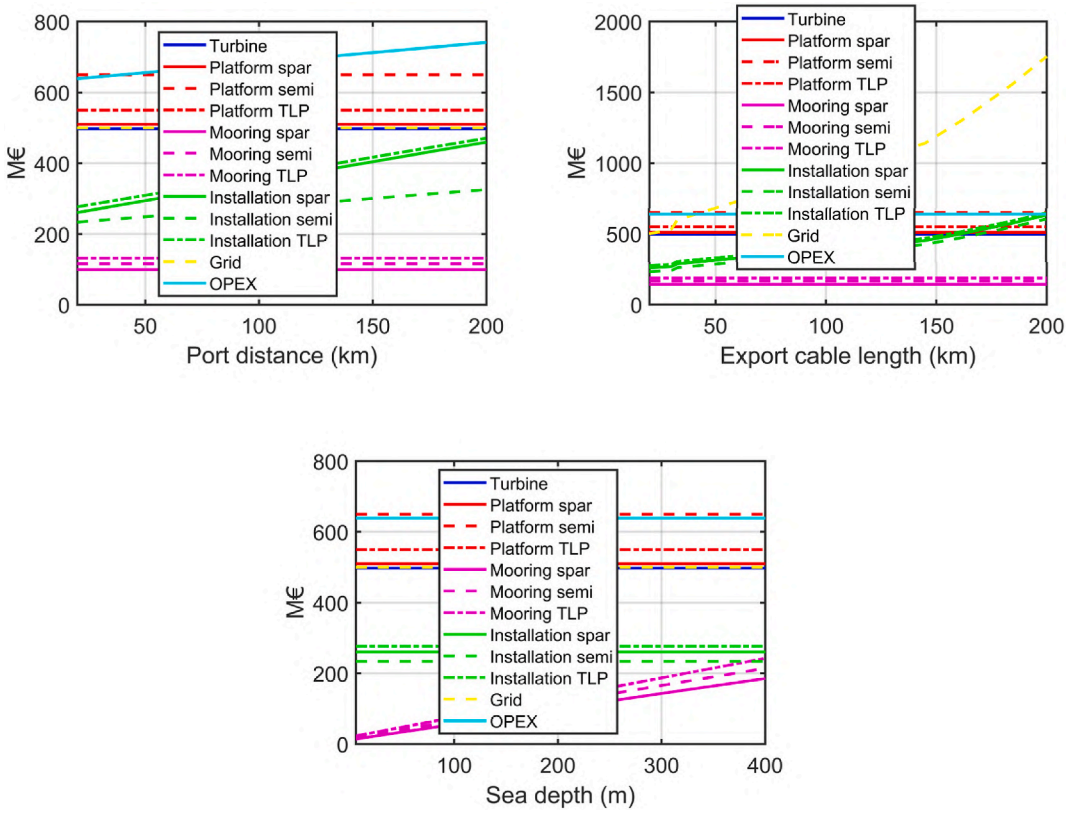

Fig. 15. Influence of the site parameters on the offshore wind farm costs for a wind farm of 100 turbines and 15 MW wind turbines. (2-columns image).

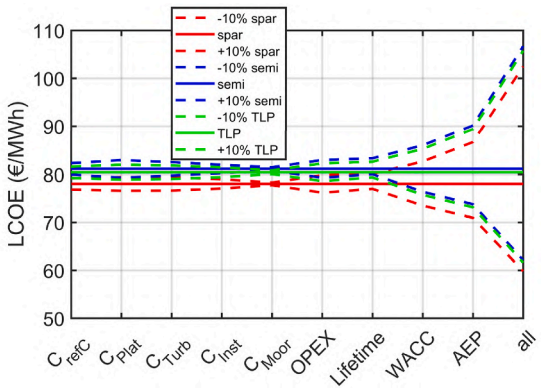

Fig. 16. Sensitivity of several offshore wind farm costs, lifetime, WACC and AEP on the LCOE. The baseline CF is assumed 30 % and it is referred to a wind farm of 100 turbines and 15 MW wind turbines. Assumed site parameters are the port and HVAC substation distance of 50 km and the water depth of 200 m. (1-column image).

platform and the maintenance will improve over the next years; the project lifetime will become longer while WACC will reduce due to the more mature technology. Fig. 16 shows the influence of a 10 % variation of several input parameters which determines a LCOE variation between 0.4 % due to the mooring and 11.1 % due to the AEP. The impact of the variation of the input parameters on the LCOE for the different types of platforms is similar. The maximum variation of the LCOE due to the combination of all the input parameters is about 31.6 % which is quite significant.

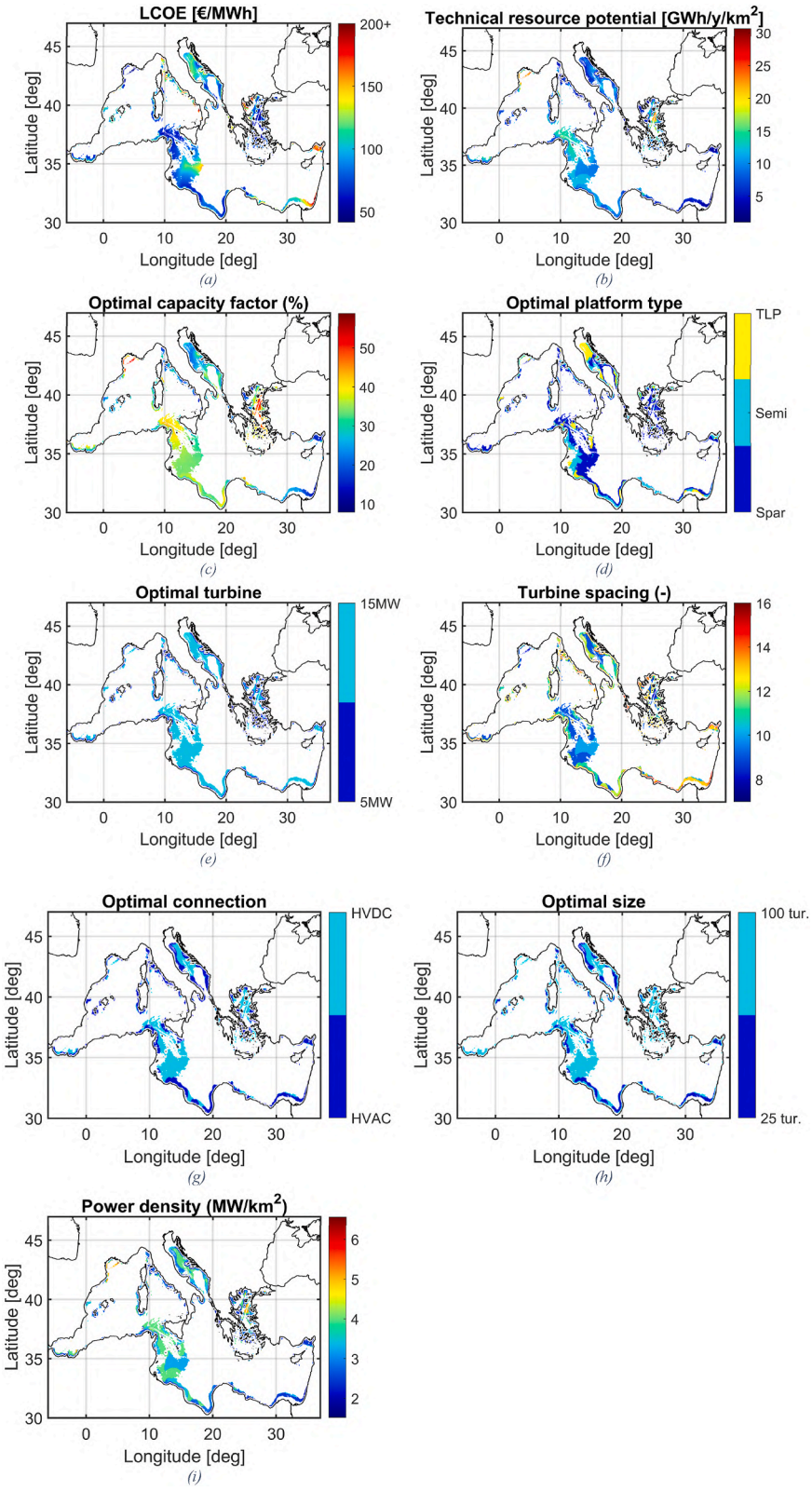

Fig. 17. Optimal LCOE (a), technical resource potential (b), capacity factor (c), platform type (d), wind turbine (e), spacing (f), grid connection (g), wind farm size (h), and power density (i) across Mediterranean Sea. (2-columns image).

3.4. Optimal floating offshore wind farms

The optimal design parameters for floating offshore wind farms in the Mediterranean Sea are shown in Fig. 17 while the most suitable design parameters are shown in Table 9. The lowest LCOE, the largest technical resource potential and capacity factors are reached in the Gulf of Lion, in the Strait of Sicily, along the coast of Libya, and in the Aegean Sea, especially next to Lesbos as shown in Fig. 17a, 17b and 17c respectively. The sea area near Lesbos is characterised by a larger distance from the coast and is, therefore, less constrained compared to other Aegean islands. LCOE and capacity factors have the highest correlation factor of 92.1 %, while there is a correlation of 83.5 % and 82.9 % between the LCOE and the distance to the onshore grid substations and between the LCOE and the water depth, respectively. Cross-correlation coefficients are obtained using the MATLAB function *xcorr*.

The semi-submerged platform shows better performance compared to the TLP for the 5 MW wind turbine due to the lower mooring costs and for larger distances from available dry docks for the 15 MW, as the installation cost for this type of platform is much lower (See Fig. 15d). The spar is mostly the best type of platform for deep sea (>150 m) due to the lowest platform cost and outperforms the other two types for most of the suitable sites (59.2 %). The semi-submerged is a better choice compared to the spar in the deep sea only in a few locations far from the dry dock such as next to Tobruk in Lybia due to the lower installation cost. The spar concept is also the only platform allowed for water depths above 400 m. This type of platform is the most occurrent optimal platform in each Mediterranean country as shown in Table 9.

The optimal wind turbine type is the 15 MW (77.9 %) as shown in Fig. 15e as the ratio between power generated and total costs is higher compared to the 5 MW wind turbine. However, the 5 MW wind turbine is selected for distances between 12 km and 20 km where only this turbine is allowed. The 5 MW wind turbine is optimal only in a few countries such as Algeria, Greece, Israel, Lebanon, and Syria due to the suitable area mostly next to the coast.

The optimal spacing is influenced by the offshore wind farm size, as a larger size is related to a smaller optimal wind farm spacing due to the larger influence of installation and grid connection costs on the LCOE. A larger spacing is obtained for the 5 MW wind turbine due to the lower costs for installation and grid connection relative to the total cost compared to the 15 MW (See Fig. 15f). Most of the Eastern Mediterranean countries have a larger optimal spacing (>10) such as Cyprus, Egypt, Israel, Lebanon, and Turkey, due to the suitable area which mostly has the smaller optimal wind farm size (25).

HVDC grid connection is preferred compared to HVAC for longer distances to the onshore grid substation such as in the deeper sea of the Strait of Sicily, in Adriatic and Aegean Seas (See Fig. 15g). The countries which have an optimal HVDC for most locations are Croatia, Greece, Libya, Malta, Morocco, and Tunisia.

Optimal wind farm size is influenced by both the wind turbine and grid connection types. 100 turbines are optimal for most sites (72 %) and especially, for the 5 MW and the HVAC connection and for the 15 MW and the HVDC connection (See Fig. 15h). 25 turbines are more suitable for the 15 MW and the HVAC connection due to lower grid connection costs. Only few countries show 25 wind turbines as an optimal design which are Albania, Egypt, and Montenegro.

The optimal installed power density varies from 1.5 MW/km^2 to 6.6 MW/km^2 and is influenced by the optimal spacing, turbine type, and wind farm size (See Fig. 15i). The highest power density values are achieved in the Gulf of Lion and off the island of Lesbos, while the average density is 3.3 MW/km2.

Finally, the most occurrent optimal design parameters in the Mediterranean Sea are the 10x10 layout with an array spacing of 9 diameters and the 15 MW wind turbine, the spar platform, and the HVDC connection (21.9 %) as shown in Table 9. In particular, an optimal wind farm with a 10x10 layout, a 15 MW wind turbine, and a HVDC connection is optimal for 48 % of the suitable Mediterranean area.

3.5. Optimal technical resource potential

The Mediterranean countries with the greatest potential for floating offshore wind are Libya, Tunisia, Italy, and Greece, accounting for about 72.2 % of the total suitable area, energy production, and installed capacity in the Mediterranean Sea (See Table 10). The total offshore wind energy production amounts to 3261 TWh/year, which is about 29.6 % of the total primary energy consumption of the Mediterranean countries. Malta has the largest ratio between total offshore wind energy potential and total country energy demand (651.7 %). Lebanon, Syria, and France have the lowest ratio of less than 5 % of offshore wind suitable area and energy production compared to total offshore available area and total energy demand respectively. France's floating offshore wind potential is particularly low, as the Gulf of Lion is mostly excluded by nature protected areas. Slovenia has no floating offshore wind potential and is not listed in Table 10. The average capacity factor is 31.8 %, while the highest average capacity factor is achieved in France (42.2 %), followed by Tunisia (37.2 %) and Greece (36.1 %). The average LCOE in the Mediterranean Sea is 93.4 €/MWh, with most Mediterranean countries having an average LCOE of less than 100 €/MWh. France has the lowest average LCOE (67.5 €/MWh) followed by Tunisia (76.7 €/MWh) and Libya (84.4 €/MWh). The Eastern Mediterranean is a less suitable region for floating wind reaching the highest LCOE in Israel, Lebanon and Turkey (>135 €/MWh). The LCOE of the most suitable countries is similar to the global average for offshore wind (76 €/MWh) estimated in the IRENA study of 2022 [76]. However, other renewable energies such as hydropower, onshore wind and solar have a lower global average (30–60 €/MWh).

Fig. 18a shows the distribution of capacity factors for each Mediterranean country. The countries with the largest variability of capacity factors are France, Greece, Turkey, and Spain (standard deviation higher than 8 %), while the countries with the most similar capacity factors are Libya, Israel and Malta (standard deviation less than 3 %). The technical potential is also influenced by the distance from the coast as shown in Fig. 18b. In general, most of the potential is located less than 50 km from the coast (about 63.3 %), due to the steep bathymetry near the coast. However, in Libya, Tunisia, and Malta, a significant part of the technical potential is located more

Table 9
Optimal design parameters for Mediterranean countries.

	Platform type	Optimal turbine (MW)	Turbine spacing	Size	Connection type
Albania	Spar	15	11	25	HVAC
Algeria	Spar	5	12	100	HVAC
Croatia	Spar	15	9	100	HVDC
Cyprus	Spar	15	14	100	HVAC
Egypt	Spar	15	13	25	HVAC
France	Spar	15	8	100	HVAC
Greece	Spar	5	9	100	HVDC
Israel	Spar	5	14	100	HVAC
Italy	Spar	15	9	100	HVAC
Lebanon	Spar	5	12	100	HVAC
Libya	Spar	15	9	100	HVDC
Malta	Spar	15	10	100	HVDC
Montenegro	Spar	15	11	25	HVAC
Morocco	Spar	15	9	100	HVDC
Spain	Spar	15	13	100	HVAC
Syria	Spar	5	11	100	HVAC
Tunisia	Spar	15	9	100	HVDC
Turkey	Spar	15	13	100	HVAC
Total	Spar	15	9	100	HVDC

Table 10
Floating offshore wind potential for Mediterranean countries [77].

	Suitable area (km^2)	% EEZ area	Production (TWh/year)	% Energy demand	Installed capacity (GW)	Capacity factor (%)	LCOE (€/MWh)
Albania	4762.3	38.3	40.1	100.3	15.5	28.9	87.6
Algeria	4270.2	3.3	39.1	5.7	14.8	29.1	87.7
Croatia	21,598.0	39.6	175.9	185.2	76.0	26.2	103.3
Cyprus	800.6	0.8	3.9	12.1	2.1	21.4	126.8
Egypt	18,545.4	10.6	89.3	8.1	45.7	22.3	121.5
France	4119.5	4.7	70.7	3.0	18.0	42.2	67.5
Greece	32,378.4	6.7	346.1	109.5	103.0	36.1	86.9
Israel	1656.8	6.8	3.7	1.2	3.1	13.3	207.1
Italy	64,473.5	12.0	538.8	31.6	206.8	28.7	96.5
Lebanon	148.3	0.7	0.6	0.6	0.4	19.0	152.6
Libya	86,027.9	23.5	866.1	455.8	288.3	34.2	84.4
Malta	25,818.0	49.4	254.2	651.7	89.0	32.6	111.6
Montenegro	3138.9	51.1	25.5	212.8	10.3	27.7	91.0
Morocco	6571.7	36.9	62.2	24.2	21.6	31.9	89.0
Spain	10,530.7	4.1	90.6	5.7	34.1	28.5	93.4
Syria	361.0	3.6	2.5	2.2	1.1	25.3	106.0
Tunisia	50,711.0	51.2	604.5	516.6	183.8	37.2	76.7
Turkey	8516.3	9.8	46.9	2.4	22.0	22.4	137.8
Total	344,428.4	13.7	3260.6	29.6	1135.5	31.8	93.4

than 50 km from the coast (>50 %). Bathymetry has a significant impact on the potential areas for floating offshore wind development, as shown in Fig. 18c. All countries show a large variability in water depths, including water depths above 400 m, for which only the Spar technology is designed. Spain, France, and Egypt show the largest variability in bathymetry (standard deviation higher than 135 m), while Croatia has the least (standard deviation about 70 m). The technical potential with LCOE below 70 €/MWh is only significant for a few countries, including Tunisia, Greece, Libya, Italy, and France, and accounts for 28.8 % of the total potential, while it is 67.5 % for LCOE below 90 €/MWh (See Fig. 18d).

4. Discussion

A comparison of the LCOE, technical potential, and available areas between this study and other works is provided in Table 11. Pantusa and Tomasicchio [11] estimated the Italian and the Mediterranean potentials three to four times lower (157/742 TWh/year) compared to this study mainly due to the lower power density assumed (1.1–3.6 MW/km^2). The suitable areas of each country are larger since the minimum distance for visual impact is 8 km instead of 12 km in this study. Furthermore, this study did not consider the constraints related to the maritime traffic and the military areas. Similar to this study, the Mediterranean Countries with the largest technical potential are Italy, Libya, Tunisia, and Greece accounting for 66 % of the total potential compared to 72 % of this study. Lu et al. [14] estimated also a low Italian technical potential of 160 TWh/year which is mainly related to the assumptions of a lower maximum coast distance of 92.6 km and water depth of 200 m compared to this study. Furthermore, Lu et al. include only small wind turbines of 2.5 MW and 3.6 MW with a lower hub height capturing less energetic wind. A similar study of Lu et al. [14] was performed

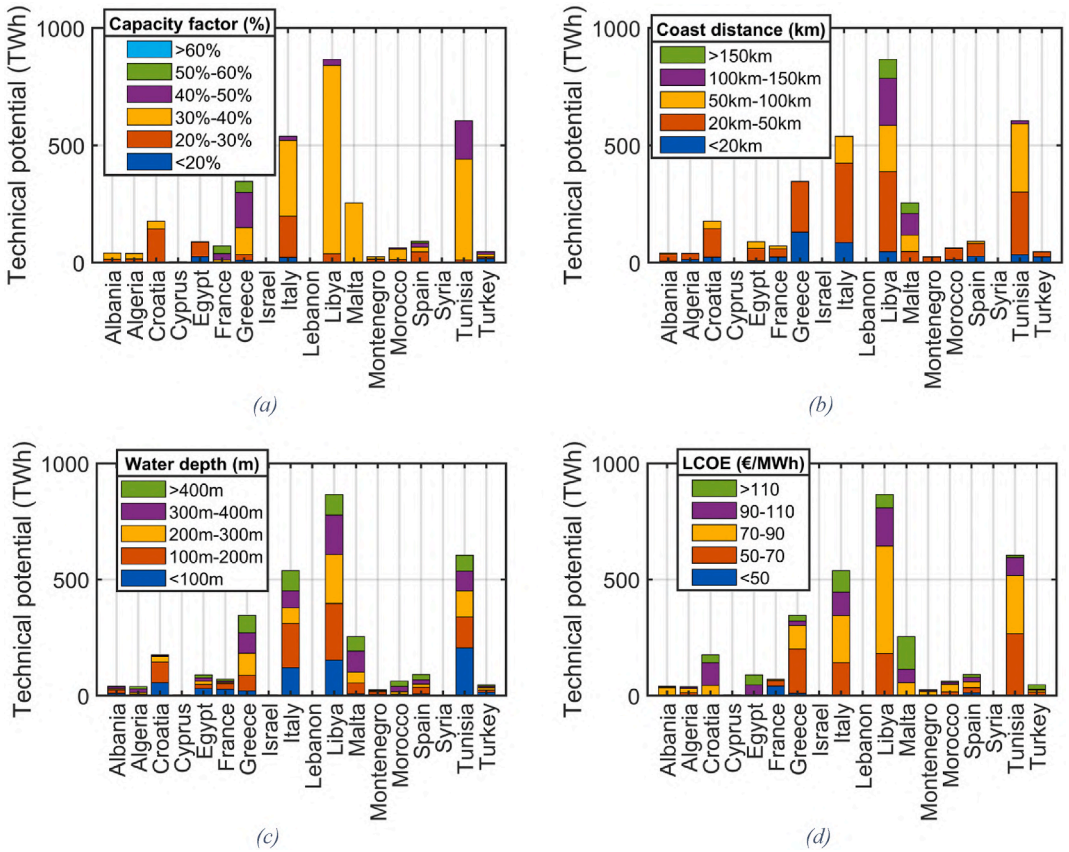

Fig. 18. Technical energy potential for different classes of capacity factor (a), distances (b), water depth (c) and LCOE (d) and for each Mediterranean Country. (2-columns image).

Table 11
Comparison of main results with other studies.

Region	This study			Other studies		
	LCOE (€/MWh)	Technical potential (TWh)	Suitable area (km^2)	LCOE (€/MWh)	Technical potential (TWh)	Suitable area (km^2)
Croatia	103.3	176	21,598	95 [10]	63 [11], 313 [10]	18,104 [10], 46,481 [11]
France	67.5	71	4120	66 [10]	12 [11], 271 [10]	9232 [11], 10,474 [10]
Greece	86.9	346	32,378	76 [10]	85 [11], 840 [10]	37,702 [10], 90,942 [11]
Italy	96.5	539	64,474	87 [10]	157 [11], 160 [14], 800 [12], 1610 [10]	83,797 [10], 134,181 [11]
Malta	111.6	254	25,818	90 [10]	26 [11], 430 [10]	22,652 [10], 32,616 [11]
Spain	93.4	91	10531	90 [10]	32 [11], 580 [10]	29,484 [11], 31,204 [10]
Gulf of Lion	51.4	n/a	n/a	57 [10], 75 [25]	202 [10]	n/a
Mediterranean	93.4	3261	344,428	n/a	742 [11]	679,331 [11]

by NREL [12] including similar assumptions. However, NREL estimated a larger technical potential of Italy of about 800 TWh compared to Lu et al. [14]. The European Commission report [10] overestimated the technical resource potential of the Mediterranean Countries compared to this study mainly due to the higher power density (7 MW/km^2) compared to this study (average 3.3 MW/km^2). The suitable areas are similar in Croatia, Greece, and Malta with a relative difference of less than 20 %, while it differs more in the other countries mainly due to the different technical limitations (maximum depth of 1000 m and minimum distance of 22 km). This study and the Energy Sector Management Assistance Program (ESMAP) study [22] show a similar installed capacity for Italy, Tunisia, and

Libya, with a relative difference of less than 12 %. This study assumed a wind farm density of 3–4 MW/km^2, water depths up to 1000 m, and a minimum wind speed of 7 m/s. A larger difference was found for Greece with an estimated potential of 413 GW compared to 103 GW in this study, as the ESMAP study covered most of the Aegean Sea and did not consider a minimum coastal distance and other constraints, such as environmental exclusion areas and maritime routes. The technical potential estimated in all these studies did not consider the environmental impact of such massive offshore wind development in the Mediterranean Sea. Maritime spatial planning is required in the Mediterranean Countries to identify the most suitable areas and allow for other maritime activities. Any floating offshore wind project should aim to minimise the environmental impact on the seabed, seabirds, and marine mammals by avoiding sensitive areas and choosing project components that reduce the impact (e.g. taut mooring, pile anchors).

Most previous studies have accounted for a constant installed power density. Dupont et al. [8] optimised the rated wind speed and the wind farm spacing parameter (1–20 rotor diameters) to maximise the net energy produced over the wind farm's lifetime obtaining an optimal power density between 0.6 and 9.3 MW/km^2. In a similar way, this study included the wind turbine spacing parameter between 4 and 30 rotor diameters. The optimal power density varied in a smaller range between 1.5 and 6.6 MW/km^2 as this study refers to the Mediterranean region compared to Dupont et al. [8] which is instead a global study and therefore a smaller variation is expected.

The average LCOE for the European Mediterranean countries of this study is similar to Ref. [10] with an average relative difference of 10.7 %. The best agreement is for France and Spain as shown in Table 11. LCOE is mainly correlated with energy production, as also reported by Martinez et al. [25], while the distance to the grid and water depth is relatively less important. In Martinez et al. a relatively higher LCOE was found compared to this study, namely 75 €/MWh in the Gulf of Lion for the best-case scenario (51 €/MWh in this study). The lower LCOE of the Gulf of Lion in this study compared to Martinez et al. could be related to the fact that Martinez et al. assumed only 5 MW wind turbines and constant aerodynamic losses (7 %) without including the optimisation of the offshore wind farm's design parameters. In contrast to other studies, this work also provides the average LCOE for the full Mediterranean basin (93.4 €/MWh).

5. Conclusion

This study investigated the floating offshore wind potential of Mediterranean countries and optimal wind farm parameters in order to provide technical guidelines for future development in the Mediterranean. The Mediterranean region is capable of producing 3261 TWh/year from floating offshore wind, which is enough to cover 29.6 % of the total energy consumption from Mediterranean countries. However, the estimation of the total technical potential is influenced by several unpredictable factors such as the visual impact and acceptance from the local population, the impact on the maritime activities (e.g. fishing sector), the electrical grid and the supply chain. Therefore, each Mediterranean country should define a maritime spatial planning strategy combined with political support for offshore wind development in order to obtain a more realistic estimate of the Mediterranean offshore wind technical potential.

The average LCOE for most Mediterranean countries is lower than 100 €/MWh, while 67.5 % of the Mediterranean technical potential has an LCOE lower than 90 €/MWh. Thus, once floating offshore wind becomes commercial, could become competitive with other renewable energies (30–60 €/MWh).

Each Mediterranean country has different optimal design parameters due to the specific offshore site conditions. The most occurrent optimal designs for floating offshore wind farms in the Mediterranean Sea are the 10x10 layout, the 15 MW wind turbine, and the HVDC connection (48 %). Hywind outperforms WindFloat and GICON-SOF in 59.2 % of the suitable areas due to the lower structure costs. WindFloat has the most competitive installation cost but also the largest structure cost while GICON-SOF has the largest installation and mooring costs. The main challenge in assessing the most suitable floater is related to the accurate estimation of the installation and maintenance costs since there are several technical assumptions which are highly dependent on the site location. Future work needs to be undertaken to assess the optimal floating offshore wind platform for the Mediterranean Sea since there are several platforms available in the market which have not been investigated. Furthermore, the floating platforms considered are not optimised yet for the Mediterranean Sea since they are designed for the ocean climate.

Irregular wind farm layouts may be included in future research to further minimise LCOE. Installation and maintenance costs can be investigated to also account for the influence of site-specific operational weather windows and several strategies. Finally, mooring costs can be also detailed to include the most suitable anchor system of each floating platform as a function of the type of seabed.

CRediT authorship contribution statement

E. Faraggiana: Writing – review & editing, Writing – original draft, Visualization, Software, Resources, Methodology, Investigation, Formal analysis, Data curation, Conceptualization. **A. Ghigo:** Writing – review & editing. **M. Sirigu:** Writing – review & editing. **E. Petracca:** Writing – review & editing. **G. Giorgi:** Writing – review & editing. **G. Mattiazzo:** Supervision, Funding acquisition. **G. Bracco:** Supervision, Funding acquisition.

Declaration of competing interest

The authors declare that they have no known competing financial interests or personal relationships that could have appeared to influence the work reported in this paper.

References

[1] K. Hainsch, H. Brauers, T. Burandt, L. Göke, C.R. von Hirschhausen, C. Kemfert, M. Kendziorski, K. Löffler, P.-Y. Oei, F. Präger, B. Wealer, Make the European Green Deal Real: Combining Climate Neutrality and Economic Recovery, DIW Berlin: Politikberatung kompakt, Berlin, 2020.
[2] European Union, Directive 2009/28/EC of the European Parliament and of the Council of 23 April 2009, Official Journal of the European Union, 2009.
[3] European Commission, REPowerEU plan. https://commission.europa.eu/strategy-and-policy/priorities-2019-2024/european-green-deal/repowereu-affordable-secure-and-sustainable-energy-europe_en, 2023. (Accessed 29 August 2023).
[4] R. Novo, P. Marocco, G. Giorgi, A. Lanzini, M. Santarelli, G. Mattiazzo, Planning the decarbonisation of energy systems: the importance of applying time series clustering to long-term models, Energy Convers. Manag. X 15 (2022) 100274, https://doi.org/10.1016/j.ecmx.2022.100274.
[5] European Commission, An EU Strategy to Harness the Potential of Offshore Renewable Energy for a Climate Neutral Future, 2020. Brussels.
[6] WindEurope, Offshore Wind Energy 2022 Mid-year Statistics, 2022.
[7] Interreg Mediterranean, Maestrale, 2020. http://maestrale-webgis.unisi.it/. (Accessed 20 July 2023).
[8] E. Dupont, R. Koppelaar, H. Jeanmart, Global available wind energy with physical and energy return on investment constraints, Appl. Energy 209 (2018) 322–338, https://doi.org/10.1016/j.apenergy.2017.09.085.
[9] D.G. Caglayan, D.S. Ryberg, H. Heinrichs, J. Linßen, D. Stolten, M. Robinius, The techno-economic potential of offshore wind energy with optimized future turbine designs in Europe, Appl. Energy 255 (2019) 113794, https://doi.org/10.1016/j.apenergy.2019.113794.
[10] I. Kielichowska, K. Staschus, A.V. Lejarreta, L. Sijtsma, L. Ramaekers, B. Vree, G.R. Yeomans, C. Wouters, S. Lindroth, F. Krönert, Study on the Offshore Grid Potential in the Mediterranean Region, 2020. Brussels.
[11] D. Pantusa, G.R. Tomasicchio, Large-scale offshore wind production in the Mediterranean Sea, Cogent Eng 6 (2019) 1661112, https://doi.org/10.1080/23311916.2019.1661112.
[12] D. Arent, P. Sullivan, D. Heimiller, A. Lopez, K. Eurek, J. Badger, H.E. Jorgensen, M. Kelly, L. Clarke, P. Luckow, Improved Offshore Wind Resource Assessment in Global Climate Stabilization Scenarios, NREL Technical Report TP-6A20-55049, Golden, CO (United States), 2012.
[13] J. Bosch, I. Staffell, A.D. Hawkes, Temporally explicit and spatially resolved global offshore wind energy potentials, Energy 163 (2018) 766–781, https://doi.org/10.1016/j.energy.2018.08.153.
[14] X. Lu, M.B. McElroy, Global potential for wind-generated electricity, Wind Energy Engineering (2017) 51–73, https://doi.org/10.1073/pnas.0904101106.
[15] R.J. Swart, C. Coppens, H. Gordijn, M. Piek, P. Ruyssenaars, J.J. Schrander, P. de Smet, M. Hoogwijk, M. Papalexandrou, E. de Visser, others, Europe's Onshore and Offshore Wind Energy Potential: an Assessment of Environmental and Economic Constraints, EEA Techical Report No 6/2009, Copenhagen, 2009.
[16] C.L. Archer, M.Z. Jacobson, Evaluation of global wind power, J. Geophys. Res. Atmos. 110 (2005), https://doi.org/10.1029/2004JD005462.
[17] L.M. Miller, A. Kleidon, Wind speed reductions by large-scale wind turbine deployments lower turbine efficiencies and set low generation limits, in: Proceedings of the National Academy of Sciences, vol. 113, 2016, pp. 13570–13575, https://doi.org/10.1073/pnas.1602253113.
[18] S. Cavazzi, A.G. Dutton, An Offshore Wind Energy Geographic Information System (OWE-GIS) for assessment of the UK's offshore wind energy potential, Renew. Energy 87 (2016) 212–228, https://doi.org/10.1016/j.renene.2015.09.021.
[19] L. Hong, B. Möller, Offshore wind energy potential in China: under technical, spatial and economic constraints, Energy 36 (2011) 4482–4491, https://doi.org/10.1016/j.energy.2011.03.071.
[20] A. Pacheco, E. Gorbeña, C. Sequeira, S. Jerez, An evaluation of offshore wind power production by floatable systems: a case study from SW Portugal, Energy 131 (2017) 239–250, https://doi.org/10.1016/j.energy.2017.04.149.
[21] A. Azzellino, C. Lanfredi, L. Riefolo, V. De Santis, P. Contestabile, D. Vicinanza, Combined exploitation of offshore wind and wave energy in the Italian seas: a spatial planning approach, Front. Energy Res. 7 (2019) 42, https://doi.org/10.3389/fenrg.2019.00042.
[22] ESMAP, Offshore wind technical potential. https://www.esmap.org/esmap_offshorewind_techpotential_analysis_maps, 2023. (Accessed 17 July 2023).
[23] T. Soukissian, F. Karathanasi, P. Axaopoulos, Satellite-based offshore wind resource assessment in the Mediterranean Sea, IEEE J. Ocean. Eng. 42 (2016) 73–86, https://doi.org/10.1109/JOE.2016.2565018.
[24] I. Balog, P.M. Ruti, I. Tobin, V. Armenio, R. Vautard, A numerical approach for planning offshore wind farms from regional to local scales over the Mediterranean, Renew. Energy 85 (2016) 395–405, https://doi.org/10.1016/j.renene.2015.06.038.
[25] A. Martinez, G. Iglesias, Multi-parameter analysis and mapping of the levelised cost of energy from floating offshore wind in the Mediterranean Sea, Energy Convers. Manag. 243 (2021) 114416, https://doi.org/10.1016/j.enconman.2021.114416.
[26] D. Pantusa, A. Francone, G.R. Tomasicchio, Floating offshore renewable energy farms. A life-cycle cost analysis at Brindisi, Italy, Energies 13 (2020) 6150, https://doi.org/10.3390/en13226150.
[27] F. Onea, E. Rusu, A spatial analysis of the offshore wind energy potential related to the Mediterranean islands, Energy Rep. 8 (2022) 99–105, https://doi.org/10.1016/j.rser.2016.08.051.
[28] M.M. Nezhad, M. Neshat, D. Groppi, P. Marzialetti, A. Heydari, G. Sylaios, D.A. Garcia, A primary offshore wind farm site assessment using reanalysis data: a case study for Samothraki island, Renew. Energy 172 (2021) 667–679, https://doi.org/10.1016/j.renene.2021.03.045.
[29] E.I. Zountouridou, G.C. Kiokes, S. Chakalis, P.S. Georgilakis, N.D. Hatziargyriou, Offshore floating wind parks in the deep waters of Mediterranean Sea, Renew. Sustain. Energy Rev. 51 (2015) 433–448, https://doi.org/10.1016/j.rser.2015.06.027.
[30] European MSP Platform, Status of MSP in the EU. https://maritime-spatial-planning.ec.europa.eu/msp-practice/countries, 2023. (Accessed 20 July 2023).
[31] Interreg Mediterranean, Maestrale, 2020. http://maestrale-webgis.unisi.it/. (Accessed 20 July 2023).
[32] Fraunhofer-Gesellschaft, ORECCA, CORDIS EU Research Results, 2011.
[33] DTU Wind Energy, Global wind Atlas. https://globalwindatlas.info/en, 2023. (Accessed 5 May 2023).
[34] ERANET+ project, New European Wind Atlas, 2023. https://map.neweuropeanwindatlas.eu/. (Accessed 13 January 2023).
[35] R. James, M.C. Ros, Floating Offshore Wind: Market and Technology Review, The Carbon Trust, 2015. https://www.carbontrust.com/our-work-and-impact/guides-reports-and-tools/floating-offshore-wind-market-technology-review. (Accessed 17 August 2023).
[36] V. Westerberg, J.B. Jacobsen, R. Lifran, The case for offshore wind farms, artificial reefs and sustainable tourism in the French mediterranean, Tour Manag 34 (2013) 172–183, https://doi.org/10.1016/j.tourman.2012.04.008.
[37] ECMWF, CERRA Sub-daily Regional Reanalysis Data for Europe on Height Levels from 1984 to Present, 2023. https://cds.climate.copernicus.eu/cdsapp#!/dataset/reanalysis-cerra-height-levels?tab=overview. (Accessed 5 May 2023).
[38] Gebco, GEBCO aims to provide the most authoritative, publicly available bathymetry data sets for the world's oceans. https://www.gebco.net/, 2022. (Accessed 10 December 2022).
[39] EMODnet, European marine Observation and data network (EMODnet). https://emodnet.ec.europa.eu/en, 2022. (Accessed 10 December 2022).
[40] Ports.com, Seaports: info, marketplace. http://ports.com, 2023. (Accessed 16 July 2023).
[41] Py PyPSA-Eur, A sector-coupled open optimisation model of the European energy system. https://zenodo.org/record/7646728#.ZFo7_BHP0uV, 2023. (Accessed 9 May 2023).
[42] G. Cervelli, L. Parrinello, C. Moscoloni, G. Giorgi, Comparison of the ERA5 wave forecasting dataset against buoy record, Instrumentation, Mesures, Métrologies 21 (2022), https://doi.org/10.18280/i2m.210301.
[43] EU, Natura 2000, 2023. https://ec.europa.eu/environment/nature/natura2000/index_en.htm. (Accessed 9 May 2023).
[44] CEMAR, Centro Tecnologico del Mar. https://cetmar.org/?lang=en, 2023. (Accessed 9 May 2023).
[45] ENTSO-E, European network of transmission system Operators for electricity. https://www.entsoe.eu/, 2023. (Accessed 9 May 2023).
[46] QGIS, A Free and Open Source Geographic Information System, 2023. https://qgis.org/it/site/. (Accessed 17 May 2023).
[47] E. Faraggiana, G. Giorgi, M. Sirigu, A. Ghigo, G. Bracco, G. Mattiazzo, A review of numerical modelling and optimisation of the floating support structure for offshore wind turbines, J Ocean Eng Mar Energy (2022) 1–24, https://doi.org/10.1007/s40722-022-00241-2.
[48] NREL, OpenFAST. https://github.com/OpenFAST, 2023. (Accessed 1 February 2023).

[49] Recharge, Gicon cleared for Baltic pilot of SOF floating wind turbine. https://www.rechargenews.com/wind/gicon-cleared-for-baltic-pilot-of-sof-floating-wind-turbine/1-1-869936, 2015. (Accessed 11 May 2023).
[50] Equinor, World's First Floating Wind Farm Has Started Production, 2023. https://www.equinor.com/news/archive/worlds-first-floating-wind-farm-started-production. (Accessed 21 July 2023).
[51] OffshoreWIND.biz, Navantia building windfloat atlantic floating foundation. https://www.offshorewind.biz/2018/08/01/navantia-building-windfloat-atlantic-floating-foundation/, 2023. (Accessed 21 July 2023).
[52] E. Faraggiana, A. Ghigo, M. Sirigu, E. Petracca, G. Giorgi, G. Mattiazzo, G. Bracco, Optimal floating offshore wind farms for Mediterranean islands, Renew. Energy 221 (2024) 119785.
[53] N.O. Jensen, A Note on Wind Generator Interaction, 1983. Citeseer.
[54] I. Katic, J. Højstrup, N.O. Jensen, A simple model for cluster efficiency, in: European Wind Energy Association Conference and Exhibition, 1986, pp. 407–410. Rome.
[55] C.N. Elkinton, Offshore Wind Farm Layout Optimization, PhD thesis, University of Massachusetts, Amherst, 2007.
[56] F. Sharkey, Offshore Electrical Networks and Grid Integration of Wave Energy Converter Arrays-Techno-Economic Optimisation of Array Electrical Networks, Power Quality Assessment, and Irish Market Perspectives, PhD thesis, Technological University, Dublin, 2015.
[57] C. Bjerkseter, A. Agotnes, Levelised Cost of Energy for Offshore Wind Turbine Concepts, Master's thesis, Norwegian University of Life Sciences, Ås, 2013.
[58] T. Wildi, Electrical Machines, Drives, and Power Systems, Pearson Educación, 2006.
[59] IEC, IEC 60228, 2023. https://webstore.iec.ch/publication/1065. (Accessed 17 January 2023).
[60] Cable Services, Cable catalogue. https://www.cableservice.com/products, 2023. (Accessed 17 January 2023).
[61] E. Giglio, E. Petracca, B. Paduano, C. Moscoloni, G. Giorgi, S.A. Sirigu, Estimating the cost of wave energy converters at an early design stage: a bottom-up approach, Sustainability 15 (2023) 6756, https://doi.org/10.3390/su15086756.
[62] E. Faraggiana, M. Sirigu, A. Ghigo, G. Bracco, G. Mattiazzo, An efficient optimisation tool for floating offshore wind support structures, Energy Rep. 8 (2022) 9104–9118, https://doi.org/10.1016/j.egyr.2022.07.036.
[63] G. Mosetti, C. Poloni, B. Diviacco, Optimization of wind turbine positioning in large windfarms by means of a genetic algorithm, J. Wind Eng. Ind. Aerod. 51 (1994) 105–116, https://doi.org/10.1016/0167-6105(94)90080-9.
[64] A. Myhr, C. Bjerkseter, A. Ågotnes, T.A. Nygaard, Levelised cost of energy for offshore floating wind turbines in a life cycle perspective, Renew. Energy 66 (2014) 714–728, https://doi.org/10.1016/j.renene.2014.01.017.
[65] A.J. Collin, A.J. Nambiar, D. Bould, B. Whitby, M.A. Moonem, B. Schenkman, S. Atcitty, P. Chainho, A.E. Kiprakis, Electrical components for marine renewable energy arrays: a techno-economic review, Energies 10 (2017) 1973, https://doi.org/10.3390/en10121973.
[66] J.F. Herbert-Acero, O. Probst, P.-E. Réthoré, G.C. Larsen, K.K. Castillo-Villar, A review of methodological approaches for the design and optimization of wind farms, Energies 7 (2014) 6930–7016, https://doi.org/10.3390/en7116930.
[67] G. Sof, A technical response to the offshore wind industry's challenges going forward, (n.d.). http://www.gicon-sof.de/en/sof1.html (accessed September 8, 2021).
[68] DTO OCEAN, Deliverable 4.6: Framework for the Prediction of the Reliability, Economic and Environmental Criteria and Assessment Methodologies for Moorings and Foundations, 2015.
[69] M. Masciola, J. Jonkman, A. Robertson, Implementation of a multisegmented, quasi-static cable model, in: The Twenty-Third International Offshore and Polar Engineering Conference, Anchorage, Alaska, 2013.
[70] A. Campanile, V. Piscopo, A. Scamardella, Mooring design and selection for floating offshore wind turbines on intermediate and deep water depths, Ocean Engineering 148 (2018) 349–360, https://doi.org/10.1016/j.oceaneng.2017.11.043.
[71] D.T.O. Ocean, Deliverable 5.6: Advanced Design Tools for Ocean Energy Systems Innovation, Development and Deployment, 2020.
[72] A.K. Dev, K.L.S. Tian, Interaction between the soil and the anchor of a semi-submersible, SNAMES (2017) 52.
[73] D. Walia, P. Schünemann, H. Hartmann, F. Adam, J. Großmann, Numerical and physical modeling of a tension-leg platform for offshore wind turbines, Energies 14 (2021) 3554, https://doi.org/10.3390/en14123554.
[74] D. Roddier, C. Cermelli, A. Aubault, A. Weinstein, WindFloat: a floating foundation for offshore wind turbines, J. Renew. Sustain. Energy 2 (2010) 33104, https://doi.org/10.1063/1.3435339.
[75] DTU, PyWake. https://topfarm.pages.windenergy.dtu.dk/PyWake/, 2023. (Accessed 1 February 2023).
[76] IRENA, Renewable Power Generation Costs in 2022, 2023. Abu Dhabi.
[77] U.S. Energy Information Administration, Energy production and consumption. https://ourworldindata.org/energy-production-consumption, 2023. (Accessed 24 July 2023).